WILEY

The impact of aquifer stratification on saltwater intrusion characteristics. Comprehensive laboratory and numerical study

Georgios Etsias[1] [iD] | Gerard A. Hamill[1] | Jesús F. Águila[1] | Eric M. Benner[1] |
Mark C. McDonnell[1] | Ashraf A. Ahmed[2] | Raymond Flynn[1]

[1]School of Natural and Built Environment, Queen's University Belfast, Belfast, UK

[2]College of Engineering, Design and Physical Sciences, Brunel University, London, UK

Correspondence
Georgios Etsias, School of Natural and Built Environment, Queen's University Belfast, Belfast, UK.
Email: g.etsias@qub.ac.uk

Funding information
Engineering and Physical Sciences Research Council Standard Research, Grant/Award Number: EP/R019258/1

Abstract

Laboratory experiments and numerical simulations were utilized in this study to assess the impact of aquifer stratification on saltwater intrusion. Three homogeneous and six layered aquifers were investigated. Image processing algorithms facilitated the precise calculation of saltwater wedge toe length, width of the mixing zone, and angle of intrusion. It was concluded that the length of intrusion in stratified aquifers is predominantly a function of permeability contrast, total aquifer transmissivity and the number of heterogeneous layers, being positively correlated to all three. When a lower permeability layer overlays or underlays more permeable zones its mixing zone widens, while it becomes thinner for the higher permeability strata. The change in the width of the mixing zone (WMZ) is positively correlated to permeability contrast, while it applies to all strata irrespectively of their relative vertical position in the aquifer. Variations in the applied hydraulic head causes the transient widening of WMZ. These peak WMZ values are larger during saltwater retreat and are negatively correlated to the layer's permeability and distance from the aquifer's bottom. Moreover, steeper angles of intrusion are observed in cases where low permeability layers overlay more permeable strata, and milder ones in the inverse aquifer setups. The presence of a low permeability upper layer results in the confinement of the saltwater wedge in the lower part of the stratified aquifer. This occurs until a critical hydraulic head difference is applied to the system. This hydraulic gradient value was found to be a function of layer width and permeability contrast alike.

KEYWORDS
angle of intrusion, aquifer heterogeneity, aquifer stratification, laboratory experiments, saline intrusion, SUTRA, toe length, width of the mixing zone

1 | INTRODUCTION

Saltwater intrusion (SWI) is initiated because of the density difference between seawater and freshwater in coastal aquifers. Projected increases in water consumption within coastal communities alongside sea level rise will intensify the phenomenon. Therefore, the study of SWI constitutes a necessary step towards facilitating the protection of freshwater reserves. Fieldwork investigations of saltwater intrusion have highlighted the impact of heterogeneous structures on the extent of saltwater intrusion (Kazakis et al., 2016; Li et al., 2009; McInnis

et al., 2013; Weinstein et al., 2007). Since real-life hydrological systems are relatively complex, their study alone is not ideal for deriving generalized conclusions about the impact of heterogeneity on saltwater intrusion characteristics. Approximations of the actual phenomenon, such as physical laboratory experiments, numerical modelling or analytical solutions have been successfully utilized instead.

The impact of aquifer heterogeneity on SWI has been investigated using predominantly analytical solutions (Ketabchi et al., 2014; Strack & Ausk, 2015) and numerical modelling (Held et al., 2005; Ward et al., 2008). Analytical solutions presented by Strack et al. (2016) indicated that a decrease in the permeability (k) of the upper part of an aquifer can significantly reduce the total length of intrusion. Expanding this study, Shi et al. (2018) conducted an analytical investigation of the impact of sea level rise on SWI in layered aquifers. This research concluded that in head-controlled systems toe length was a function of the relative hydraulic conductivities between layers. Rathore et al. (2018) introduced a new parameter, called transmissivity centroid elevation (TCE), to better evaluate the effect of stratification in SWI characteristics. TCE was defined as the summation of the product of the transmissivity and elevation (above the aquifer base) of each layer divided by the total aquifer transmissivity. Utilizing an analytical solution, it was concluded that for the same values of aquifer transmissivity, higher TCE values corresponded to longer toe length in head-controlled systems. Lu et al. (2013) conducted a numerical evaluation of the impact of stratification in the values of steady-state width of the mixing zone (the dispersion zone where the salinity of water varies from zero to 100%). Based on a setup of three-layered aquifers, it demonstrated that when a low permeability layer overlies a relatively high-k layer, the mixing zone in the low-k layer is widened. Mixing zone gets thinner in cases where highly permeable layers overlie less permeable ones.

Sandbox laboratory setups have been extensively utilized to study the fundamental mechanisms of saltwater intrusion in coastal aquifers (Abdoulhalik et al., 2017; Armanuos et al., 2019; Goswami & Clement, 2007; Konz et al., 2008; Kuan et al., 2012; Liu et al., 2017; Robinson et al., 2016; Stoeckl & Houben, 2012; Takahashi et al., 2018; Zhang et al., 2002). The majority of laboratory studies have recreated SWI in homogeneous synthetic aquifers (Abdelgawad et al., 2018; Abdoulhalik & Ahmed, 2018a, 2018b; Q. Chang et al., 2019; Guo et al., 2019; Kuan et al., 2019; Lee et al., 2019; Levanon et al., 2019; Memari et al., 2020; Na et al., 2019; Noorabadi et al., 2017; Shen et al., 2020; Stoeckl et al., 2019; Yu et al., 2019). Nevertheless, sandbox setups have been successfully employed to study freshwater—saltwater interface in aquifers with structured— sedimentary heterogeneity (Houben et al., 2018), in freshwater lenses, located in heterogeneous island aquifers (Dose et al., 2014; Stoeckl et al., 2015), as well as inside fractured porous media (Etsias et al., 2021). Regarding layered coastal aquifers in particular, the impact of stratified heterogeneity has been studied in correlation with a series of different phenomena. Liu et al. (2014) and Guo et al. (2019) studied SWI in tidally affected stratified aquifers, similarly Dalai et al. (2020) quantified the impact of shore slope, while Vithanage et al. (2012) investigated aquifer salinization due to a tsunami-like event. Similarly,

Mehdizadeh et al. (2014), studied saltwater - freshwater interface on confined aquifers with impermeable strata, Abdoulhalik and Ahmed (2017a, 2017b) evaluated the suitability of various coastal protection techniques in layered hydrological systems, while Abdoulhalik et al. (2020), investigated the impact of freshwater abstraction in heterogeneous coastal aquifers.

To the best of our knowledge, there has never been, a laboratory-based study quantifying the impact of stratification on all three fundamental saltwater intrusion characteristics, namely the toe length (TL), width of the mixing zone (WMZ) and the angle of intrusion (AOI). Although a few experimental studies were presented in the literature, those were based on steady state conditions (Lu et al., 2013) or were focusing on the effect of cut-off wall barriers (Abdoulhalik & Ahmed, 2017a). Unlike previous experimental studies that relied on simple visual observation of the sandbox data, the present investigation utilized the automated image processing techniques developed in Queen's University Belfast (Etsias, Hamill, Benner, Aguila, McDonnell, Ahmed, & Flynn, 2020a; Etsias, Hamill, Benner, Aguila, McDonnell, & Flynn, 2020b; Robinson et al., 2015). This has enabled the accurate reproduction of laboratory saltwater concentration fields, as well as the quantification of specific saltwater intrusion characteristics (TL, WMZ and AOI) with high accuracy. All the laboratory results were successfully recreated using numerical simulations. The trends identified based on the analysis of the sandbox data, were further expanded using numerical simulations, through six sensitivity analysis scenarios. The main novel aspects of this study can be summarized as follows:

- With a total of nine investigated aquifers, this is, to date, the most comprehensive laboratory study on the impact of stratification on saltwater dynamics. The direct comparison of saltwater hydrodynamics in different heterogeneous setups, enabled the identification of a series of new conclusions that have never been presented before.
- This is the only sandbox study incorporating high precision quantification of the experimental WMZ into each specific permeability layer of stratified aquifers. Supplementary to that, it assessed, for
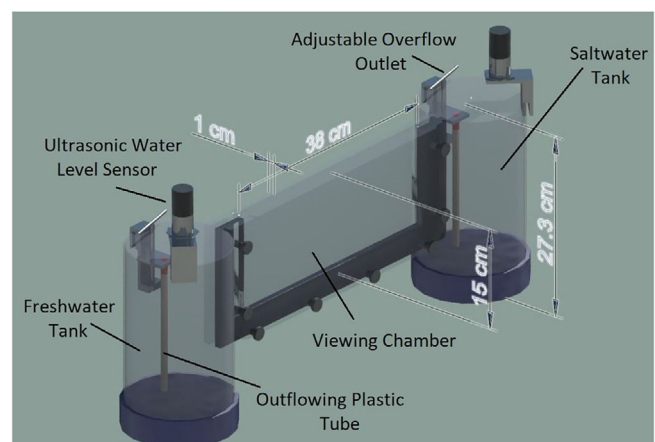

FIGURE 1 3D representation of the utilized experimental setup

the first time ever in a heterogeneous aquifer setup, the variation of WMZ under transient conditions.

- The impact of aquifer stratification on the AOI, was investigated for the first time in this study, under both steady state and transient conditions.

- The numerical sensitivity analysis identified the impact of four distinct aquifer characteristics: permeability contrast between strata; total aquifer transmissivity; total number and width of individual permeability layers. The effect of those four variables on saltwater intrusion dynamics was studied in isolation from one
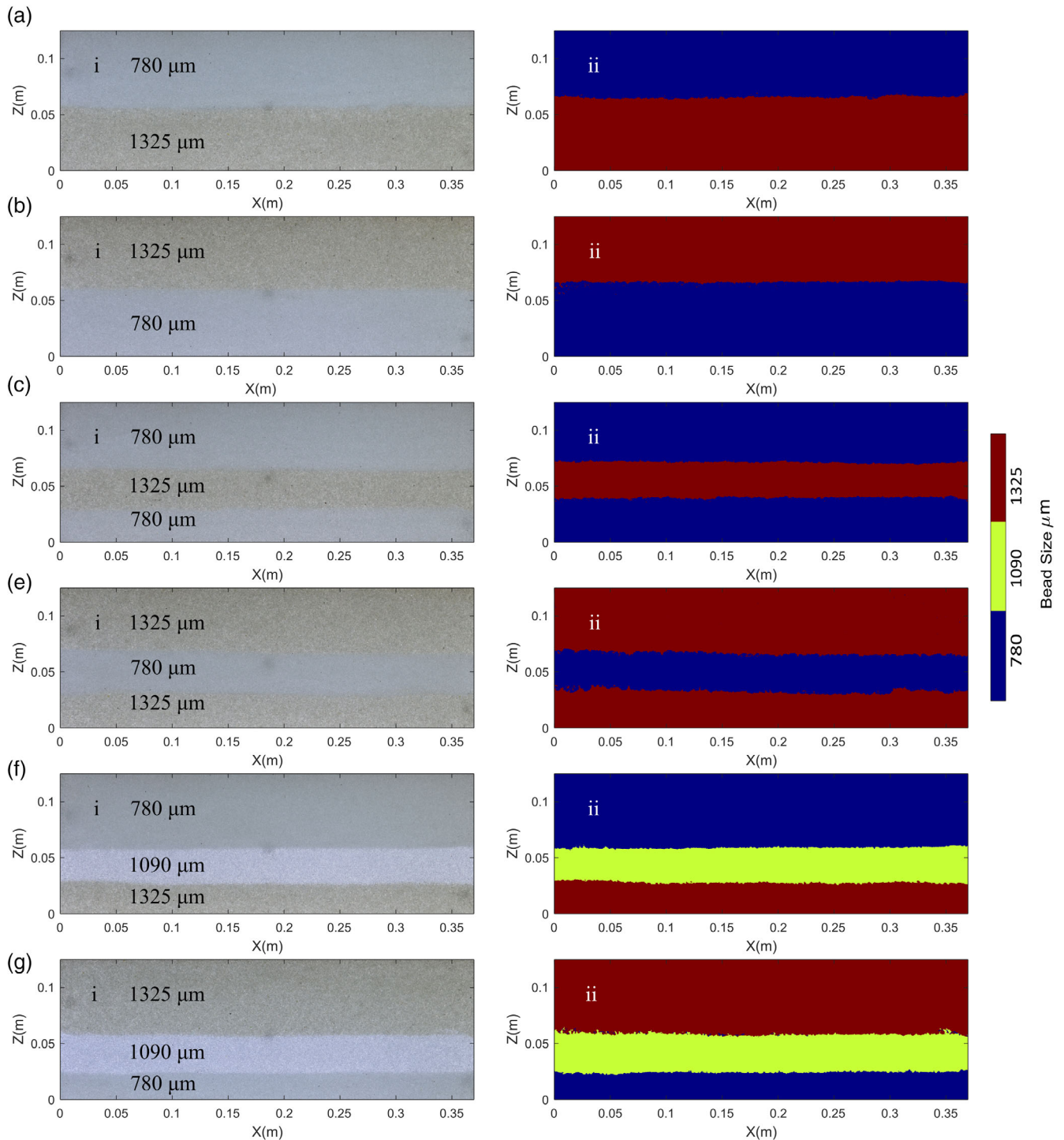

FIGURE 2 (i) Photographs and the equivalent (ii) heterogeneous structure fields (generated by the classification artificial neural network) of the six investigated stratified aquifers

another using numerical modelling. This is an element that was not taken into account in previous numerical investigations and has enabled the further expansion of the currently accepted concepts of SWI.

The conclusions of this study, derived for idealized two-dimensional laboratory experiments, should be a valuable contribution towards better understanding of SWI dynamics in real life layered aquifer systems.

2 | LABORATORY SETUP AND TEST CASES

The laboratory setup utilized to derive the experimental data of the current investigation was described in detail by Robinson et al. (2015). The sandbox apparatus consisted of a 0.38 m × 0.15 m × 0.01 m viewing chamber flanked by two cylindrical reservoirs (Figure 1). The left tank was filled with freshwater, while dyed saltwater filled the right one. Head level in the side reservoirs was monitored by two ultrasonic sensors, while adjustable outflows enabled the application of different hydraulic gradients. Glass beads of three different diameters, 780, 1090, and 1325 μm, were siphoned into the viewing chamber to minimize the amount of air trapped inside the porous medium and ensure saturated conditions. Acrylic mesh screens stabilized the beads into the central chamber. Experiments were conducted in a dark room where illumination was provided by two LED light panels positioned on the back of the laboratory rig. High resolution multi-colour images were acquired every 5 min with a Nikon D850 DSLR Camera.

Nine experimental aquifers were investigated, including three homogeneous aquifers, one for every bead size used, and six layered heterogeneous ones (Figure 2). The setup of the stratified aquifers enabled the study of various degrees of heterogeneity. The investigated layered aquifers can be divided into three categories:

- Two-layered aquifers: in the first a low permeability layer overlaid a higher permeability one (780–1325 μm), while in the second the reverse setup applied where 1325 μm high permeability

TABLE 1 Duration of laboratory experiments in minutes

Aquifer	dH = 6 mm	dH = 4 mm	dH = 5 mm
L	45	50	60
M	25	40	45
H	25	45	55
L-H	35	45	45
H-L	50	60	70
L-H-L	45	90	60
H-L-H	35	50	55
L-M-H	25	60	45
H-M-L	35	55	65

stratum was laid on top of the 780 μm low-k layer (Figure 2 (a),(b)).

- Three-layered aquifers in which a lower (1325-780-1325 μm) or higher (780-1325-780 μm) permeability middle layer intersected an otherwise homogenous aquifer (Figure 2(c),(d)).
- Three-layered aquifers in which bead size either monotonically increased (780-1090-1325 μm) or decreased (1325-1090-780 μm) in each heterogeneous layer setup (Figure 2(e),(f)).

In all tested aquifers the various strata were formed by glass beads of similar size. The layers created by the 780 μm glass beads were characterized by low (L) permeability, the 1090 μm layers by medium permeability (M) and the 1325 μm ones by high (H) permeability. In the interests of clarity, the six laboratory heterogeneous aquifers will be henceforth referred to according to the qualitative characterization of their layers' permeability, starting from the upper most stratum: L-H (Figure 2(a)), H-L (Figure 2(b)), L-H-L (Figure 2(c)), H-L-H (Figure 2(d)), L-M-H (Figure 2(e)), H-M-L (Figure 2 (f)). Similarly, the three homogeneous aquifers will be referenced as L, M and H.

Initially the aquifer contained only freshwater. Three hydraulic head level differences (dH) were applied between the fresh and saltwater tanks. A head difference of 6 mm was applied to the system triggering the initial stage of saltwater intrusion. Subsequently, the head difference decreased (4 mm) resulting in a new phase of intrusion. Finally, saltwater retreat was initiated by an increase of the hydraulic head difference (5 mm). The hydraulic gradients investigated here are within the range of hydraulic gradients observed in some real world problems (Attanayake & Sholley, 2007; Ferguson & Gleeson, 2012). During the experiment, water in the right cylinder was monitored using a YSI Professional Plus Instrument (Pro Plus) water quality meter; this ensured that salinity did not reduce due to the outflow of freshwater through the porous medium. Total data acquisition time per intrusion or retreat phase varied from 50 to 90 min (Table 1), depending on the aquifers' heterogeneous structure.

Experimental images were post-processed using the machine learning oriented method introduced by Etsias, Hamill, Benner, Aguila, McDonnell, and Flynn (2020a). A multi-layered classification artificial neural network (ANN) was utilized to precisely recognize the heterogeneous structure of the six stratified aquifers (Figure 2). Subsequently, saltwater concentration fields were generated for all the steady-state saltwater intrusion images (dH = 6, 4 and 5 mm) by a 10-neuron regression ANN with one hidden layer (Figure 3). The values of specific saltwater intrusion variables such as toe length of intruding wedge, width of mixing zone and angle of intrusion were calculated for the derived concentration fields by applying the data processing algorithms presented by Robinson et al. (2015). TL quantifies the extent of saltwater intrusion, which was determined as the distance of the 50% saltwater concentration isoline from the right (saltwater) edge of the laboratory aquifer. WMZ equalled to the average vertical distance between the 25% and 75% salinity isolines, while the AOI is the angle that the saline wedge formed with the bottom of the aquifer, or with the interface of different permeability layers.
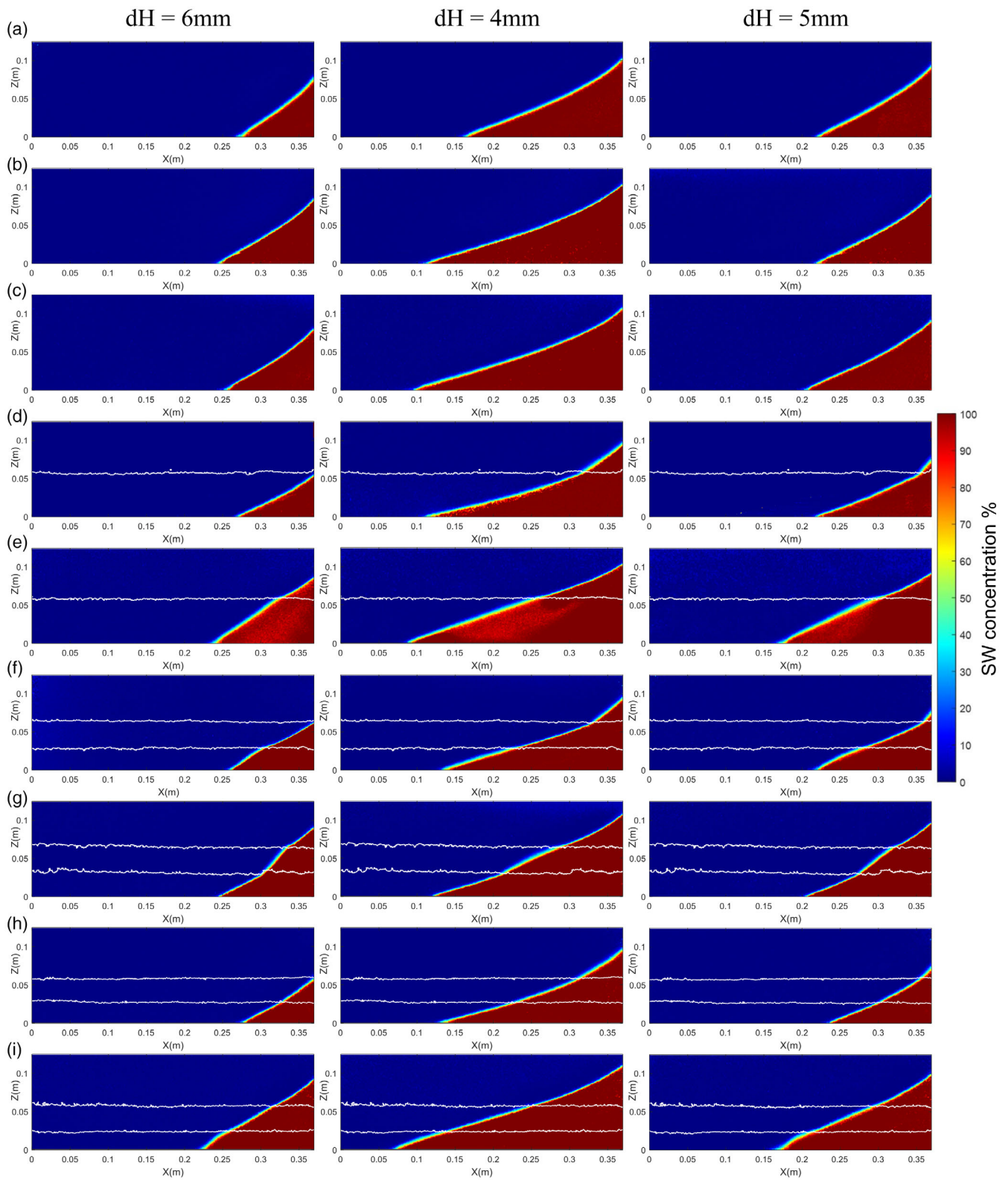
FIGURE 3 Experimental steady state saltwater concentration fields of the (a) L, (b) M, and (c) H homogeneous, and the (d) L-H, (e) H-L, (f) L-H-L, (g) H-L-H, (h) L-M-H and (i) H-L-M heterogeneous aquifers

3 | NUMERICAL MODELLING

Numerical simulations using the density-dependent flow and transport code SUTRA (Voss & Provost, 2010) were conducted to assess the consistency of the experimental setup by successfully recreating the acquired laboratory data. Furthermore, numerical modelling was utilized for the execution of a rigorous sensitivity analysis aiming to further quantify the impact of stratification on the various saltwater intrusion characteristics (TL, WMZ and AOI).

Two-dimensional models with a size of 0.38 m × 0.134 m were created. The model domain was discretized with a uniform 2-D finite element mesh with square elements with a size of 1.22×10^{-3} m. The element size and aquifer dispersivity (longitudinal dispersivity = 10^{-3} m, transverse dispersivity = 3.75×10^{-5} m) have satisfied Peclet number criterion (Voss & Souza, 1987). Hydrostatic pressure was specified at the right (saltwater) and left (freshwater) boundaries of the model to simulate the head level differences of 6, 4 and 5 mm. An intrinsic flow test on the experimental domain allowed the calculation of the permeability of the porous media using Darcy's law. Saturated-unsaturated groundwater flow models were performed since similar models have been successfully utilized before to simulate saltwater intrusion occurring in a sandbox setup (Houben et al., 2018). In this study, the van Genuchten equation (van Genuchten, 1980) was used to simulate the unsaturated flow. The van Genuchten parameters of the numerical model were derived from experimental data for

TABLE 2 Summary of the numerical parameters

Input parameters		Values
Domain length (m)		0.38
Domain height (m)		0.134
Element size (m)		1.22×10^{-3}
Permeability (m^2)		
780 μm		7.98×10^{-10}
1090 μm		1.83×10^{-9}
1325 μm		2.39×10^{-9}
Van Genuchten parameters:	α (1/Pa)	n
780 μm	6.9×10^{-4}	7.58
1090 μm	8.45×10^{-4}	4.5
1325 μm	9.63×10^{-4}	2.17
Porosity		0.385
Long. dispersivity (m)		10^{-3}
Trans. dispersivity (m)		3.75×10^{-5}
Freshwater density (kg/m^3)		1000
Saltwater density (kg/m^3)		1025
Freshwater head (m)		0.134
Saltwater head (m)		0.128–0.13
Time step (sec)		1
Simulation time (min)		
Simulating exp. aquifers		50–90
Sensitivity analysis		60

glass beads of comparable size (Benson et al., 2014; Sweijen et al., 2017). The values of applied dispersivities conformed to the range determined by Abarca and Clement (2009). Model input parameters are summarized in Table 2. The simulation time for each recreated laboratory case was identical to the equivalent experimental duration, while the time-step was equal to 1 s.

The study was expanded via sensitivity analysis that evolved around six simulation scenarios. The total simulation time for each intrusion and retreat phase on these scenarios was 60 min. During this period, steady state was achieved in all numerical cases. The layer permeability values used here were kept similar to those measured in the laboratory setup. In none of the simulations did the utilized permeability values vary more than an order of magnitude from the experimental ones. To better visualize the correlation between the SWI characteristics and aquifer stratification variables, nonlinear fitting was applied between the numerical results in all scenarios. Since formulating precise generalized equations was beyond the scope of this study, power law was the basis for the conducted interpolations, and the data fit was deemed satisfactory in all cases. For the sake of clarity, these scenarios are presented alongside the experimental and numerical results in Section 4. The heterogeneous structure of the layered aquifers investigated during the six sensitivity analysis scenarios is presented in detail in the Appendix S1.

4 | RESULTS AND DISCUSSION

4.1 | Experimental results

The experimental steady-state saltwater concentration fields of the nine investigated aquifers are presented in Figure 3. The laboratory data were successfully reproduced with numerical simulations, during both the two intrusion and the final saltwater retreat phase (Figures 4 and 5 and A1 of the appendix). In contrast to the homogeneous aquifer settings, experimental saltwater wedges in the layered cases demonstrated significant refraction at the freshwater-saltwater interface. The general shape of the simulated saltwater wedges as well as the specific saltwater characteristics that is, TL, WMZ and AOI exhibited a high quality fit with the experimental data, nevertheless some variation could still be identified. The TL values generated by the utilized numerical model (Figure 5) were comparable to the experimental TLs for the initial intrusion (dH = 6 mm) and the final retreat phase (dH = 5 mm), presenting an average relative difference of 5.3% and 4.8% respectively. During the second intrusion phase (dH = 4 mm) the numerical model underpredicted the extent of saline intrusion by an average of 9.7%, while the difference between experimental and numerical results was the greatest for the H-M-L aquifer (5.6 cm). Similarly, the numerical saltwater concentration fields in the H-L aquifer (Figure 4(b)) included a far thinner mixing zone inside the low permeability stratum than its equivalent experimental field.

In sandbox setups of relatively small size, experimental errors can be introduced by flaws in water level adjustment and sandbox levelling, as well as by uneven flow through the side mesh screens or

variations in the density of the saline solution. Moreover, minor heterogeneities due to small variations in the diameter of glass beads and packing may exist in the experimental settings while not accounted for in the numerical model, which assumes perfect homogeneity for each bead layer. Automated image analysis algorithms were employed

in this study to determine the boundaries between the layers. Nevertheless, since the size of utilized elements was similar to that of a single glass bead, there was some divergence between the generated numerical and experimental permeability fields. Finally, numerical TL underprediction, of comparable scale, has been reported in previous
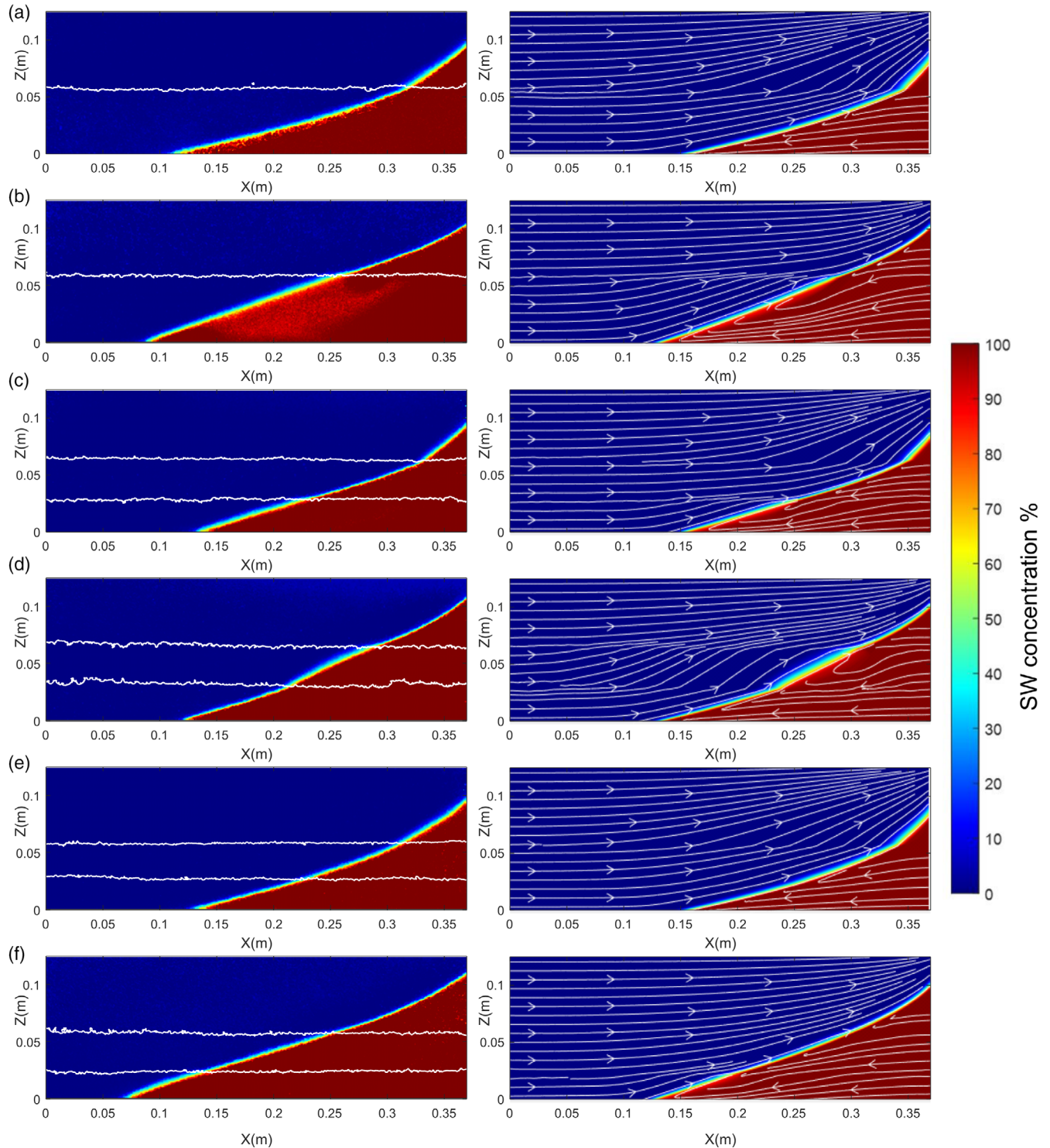

FIGURE 4 Experimental (left) and numerical (right) steady state saltwater concentration fields of the (a) L-H, (b) H-L, (c) L-H-L, (d) H-L-H, (e) L-M-H and (f) H-M-L stratified aquifers. Saline intrusions initiated by a hydraulic head difference of 4 mm
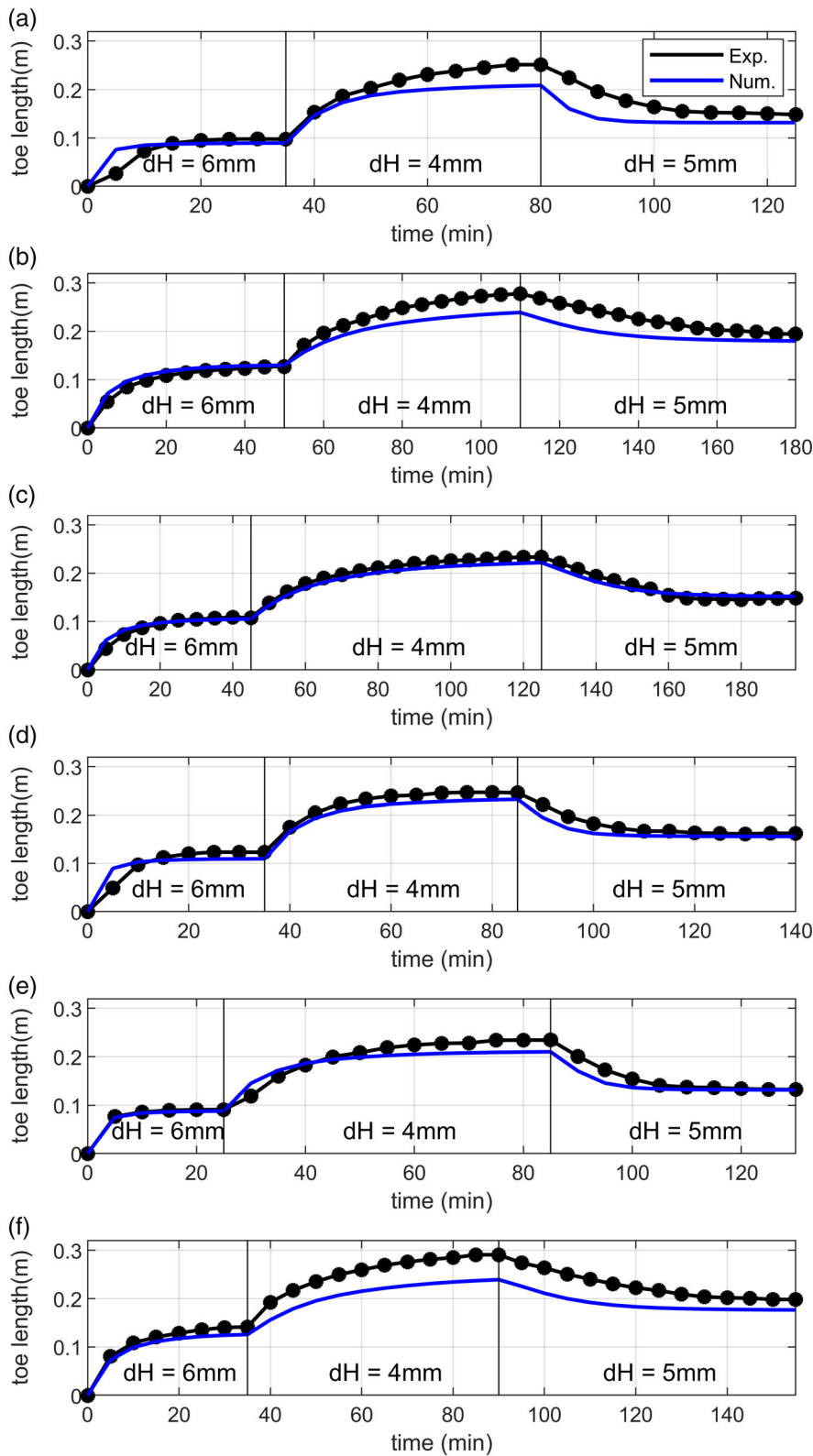
FIGURE 5 Experimental and numerical transient toe length values of the (a) L-H, (b) H-L, (c) L-H-L, (d) H-L-H, (e) L-M-H and (f) H-M-L μm stratified aquifers

laboratory studies (Abdoulhalik & Ahmed, 2017a and 2018a). Despite this limited variance between experimental and numerical data, the numerical model, being successfully benchmarked against a large amount of detailed experimental data, can be reliably utilized to

further investigate the impact of aquifer stratification on saltwater intrusion characteristics.

The simulated velocity vector fields for the six heterogeneous laboratory aquifers are presented in Figure 6. In addition to validating
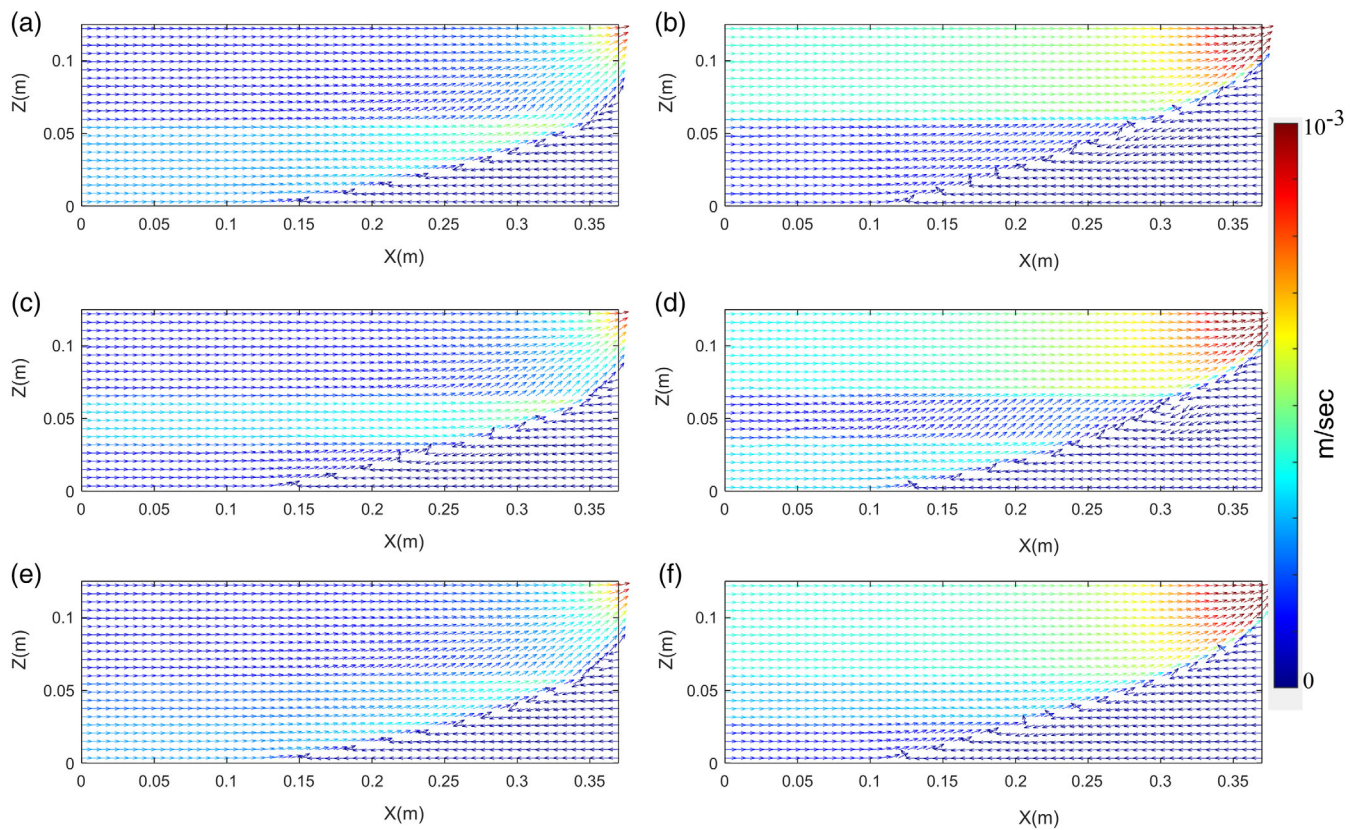
FIGURE 6 Flow velocity vector fields, generated by a hydraulic head difference of 4 mm for the (a) L-H, (b) H-L, (c) L-H-L, (d) H-L-H, (e) L-M-H and (f) H-M- heterogeneous aquifers

the experimental data, numerical simulations provided an insight on the main driving force prompting the SWI characteristics observed in the laboratory images. Figures 4 and 6 outlined the direction and magnitude of flow velocities inside the stratified aquifers. Due to the density difference between the two fluids, freshwater overtops saltwater, which intrudes underneath it. As expected, in all the investigated setups, flow velocities inside the saline wedges were considerably lower than those of the freshwater, (Chang & Clement, 2012). Freshwater velocity was in turn greatly affected by the permeability of the various layers. This permeability contrast resulted in sharp variation in both the direction and magnitude of the flow velocity vectors at the interface between different layers. Streamline refraction is the change in the direction of water flowing from one permeability zone to another and is represented by the injection and refraction angles. Injection angle indicates the direction of streamlines outflowing from a layer is equal to the angle that the streamline forms with the plane that is perpendicular to the interface of the two strata. Similarly, refraction angle expresses the flow direction into another layer. When water entered a low permeability layer from a more permeable one, refraction angles were smaller than injection angles, resulting in steeper streamlines and vice versa. In the head driven systems used here, outflow occurred at the upper right part of the aquifers. Velocities around the outflow zone were relatively higher than those in the rest of the system, especially in cases where the upper layer exhibited a higher permeability (H).

The acquired experimental data allowed novel concepts about the impact of stratification on SWI to be formulated and subsequently expanded through rigorous sensitivity analysis. The effect of stratification on each one of the main SWI characteristics is now presented.

4.1.1 | Toe length

For all experimental images, the toe length was inversely correlated to the applied hydraulic head difference, which is in agreement with previous investigations (Houben et al., 2018). The lengths of the experimental saltwater wedges initiated by a 4 mm head difference are presented in Figure 7. The intruding wedge size exhibited a small variation between the three investigated homogeneous aquifers, being the shortest in the lower permeability aquifer. This reproduces the experimental correlation between average aquifer permeability and TL in homogeneous aquifers reported by Robinson et al. (2016). Saltwater intrusion was more pronounced in heterogeneous aquifers when high permeability layers overtopped the lower permeability ones as in the aquifer configurations H-M-L, and H-L, while the TL was considerably shorter in the inverse heterogeneous setups (L-M-H, L-H). The overlaying, less permeable zone forced the freshwater to flow through the lower high-permeability layer at a greater velocity (Figure 6), enhancing the repulsion of the saltwater wedge, pushing it back towards the seaside boundary. The results are in agreement with
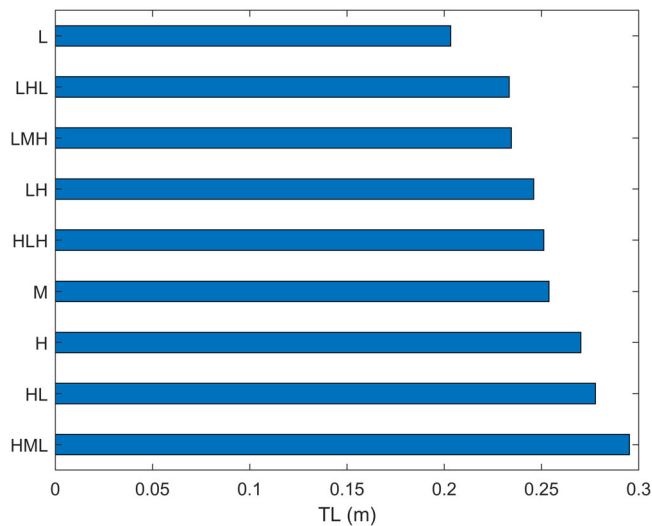
FIGURE 7 Experimental toe length of intruding wedge initiated by a hydraulic head difference of 4 mm for the nine investigated aquifers

TABLE 3 Average aquifer permeability and TCE of the six heterogeneous experimental aquifers

Aquifer	Avg. aquifer permeability (m^2)	TCE (cm)
L-H	1.53E-09	4.63
H-L	1.65E-09	7.74
L-H-L	1.25E-09	5.67
H-L-H	1.96E-09	6.56
L-M-H	1.40E-09	4.68
H-M-L	1.94E-09	7.2

Abbreviation: TCE, transmissivity centroid elevation.

previous experimental (Abdoulhalik and Ahmed, 2017a and b), analytical (Strack et al., 2016) and numerical (Shi et al., 2018) studies.

These two basic concepts about the effect of hydraulic gradient and the distribution of permeability layers may not be sufficient to accurately predict which aquifer would exhibit the most extended SWI. A novel variable, TCE, was introduced by Rathore et al. (2018) to quantify the impact of stratification on SWI. TCE values alongside average aquifer permeability were calculated for the six heterogeneous experimental aquifers (Table 3) using the following equations:

$$k_{\mathrm{avg}} = \frac{\sum_{i=1}^{n}(k_i \times b_i)}{b_{\mathrm{total}}}, \quad (1)$$

$$\mathrm{TCE} = \frac{\sum_{i=1}^{n}(k_i \times y_i)}{k_{\mathrm{avg}}}, \quad (2)$$

where n is the number of layers, k is permeability, b is layer width and y is layer elevation above the aquifer's base.

The laboratory data indicated that aquifers with higher TCE and average permeabilities manifested longer saline wedges (Table 3). Even though TCE was formulated using idealized steady state analytical solutions, which assumed a sharp interface between freshwater and saltwater, the current investigation evidences its validity under controlled laboratory conditions, where dispersive approach applies and the assumptions of analytical solutions do not exist. Nevertheless, TCE values alone could not sufficiently determine which aquifer would exhibit the longest TL. This indicated that the real-world phenomenon is more complex than the analytical and numerical approximations that have been tested up to now. Sensitivity analyses were undertaken to investigate the impact of: permeability contrast between layers (Scenario 1), total aquifer transmissivity (Scenario 2) and the number of heterogeneous layers

(Scenario 3) in the steady state length of intrusion. Unlike all previous investigations, in this sensitivity analysis, the three aforementioned heterogeneity characteristics were studied in isolation from each other in order to successfully quantify their impact on the extent of saline intrusion (TL).

4.1.2 | Width of the mixing zone

Changes in the width of the mixing zone from layer to layer were easily detectable through visual observation of the post-processed laboratory concentration fields (Figure 3). Higher permeability layers showed a thinner mixing zone, while low permeability layers had a wider one, caused by more intense dispersion and diffusion effects (Abdoulhalik & Ahmed, 2017a). This applied to homogeneous and heterogeneous cases alike. The impact of layered heterogeneity on WMZ was investigated through numerical simulations by Lu et al. (2013). The basic finding of this study was that when a low permeability aquifer overlies a relatively high-k layer, the mixing zone in the low-k layer is widened. It is worth clarifying that according to Lu et al. (2013), the change of the mixing zone applied only for the overlying layer.

This phenomenon, observed up to now in idealized steady state numerical simulations, was successfully identified on a laboratory scale for the first time in this study. Moreover, the advanced image analysis algorithms utilized, allowed the precise quantification of the experimental variation in WMZ values, for each permeability layer. The mixing zone in the middle layer of the H-L-H aquifer was 0.44 cm, wider than that of the corresponding low permeability (L) homogeneous aquifer, in which WMZ was equal to 0.40 cm. Similarly, WMZ in the middle layer of the L-H-M aquifer was thinner (0.15 cm) than that of the H homogeneous aquifer (0.24 cm). Experimental values of WMZ for the 780 μm (L) and 1325 μm (H) bead size layers of all the experimental aquifers are listed in Table 4. It is evident that in all the heterogeneous cases, WMZ of the L layers was wider than that of the equivalent L homogeneous aquifer, while for the H bead size WMZ decreased. These data expand the conclusion of Lu et al. (2013) that identified this variation of WMZ strictly on the upper—

TABLE 4 Experimental width of the mixing zone in high (H) and low (L) permeability layers of saltwater wedges initiated by 4 mm hydraulic head difference

Target layer	Aquifer	WMZ(cm)
High permeability layer	H	0.34
	L-H	0.30
	L-M-H	0.27
	H-M-L	0.24
	H-M-L (bottom)	0.23
	H-M-L (top)	0.22
	H-L	0.22
	H-L-H	0.20
Low permeability layers	L-H	0.57
	L-M-H	0.51
	H-L	0.50
	H-L-H	0.50
	L-H-L (top)	0.43
	L-H-L (bottom)	0.42
	H-M-L	0.42
	L	0.40

overlaying stratum. Instead, they indicate that that when a low permeability layer borders a higher permeability layer, either overlying or underlying it, its mixing zone widens. The opposite phenomenon occurs for the mixing zone of higher-k layers.

Flow refraction at the interface of two layers of different permeability can either condense or isolate the flow streamlines. According to conservation of mass, the separation of streamlines results in the widening of the mixing zone. On the other hand, the presence of crowded streamlines corresponds to less mixing between fresh and saltwater. The variations of WMZ, observed in the laboratory data, can be partly attributed to this previously documented mechanism (Lu et al., 2013). The impact of stratification on steady state WMZ was further quantified via sensitivity analysis using numerical simulations (Scenario 4).

The transient values of the WMZ in the six stratified aquifers, during the whole duration of the experiment, are presented in Figure 8. It is evident, that the steady state WMZ values in each permeability layer do not demonstrate significant variation for the three different hydraulic gradients applied in the aquifer. On the other hand, every change on the dH was succeeded by a distinct transient widening of the mixing zone, which occurred during both the saltwater intrusion and retreat phases of the experiment. This variation in WMZ was significant during the initial intrusion of the saline wedge in each individual permeability layer. On the other hand, it was observable, but relatively limited, during the second intrusion phase, where dH decreased from 6 to 4 mm, while it was greatest in the final retreat stage of the experiment (dH = 4 – 5 mm). These findings agree with previous laboratory scale observations of SWI in homogeneous aquifers (Robinson et al., 2016).

Since the widening of the mixing zone was greater in the saltwater retreat (SWR) phase, the quantitative analysis of transient WMZ values, focused on the data generated from this final stage of the experimental observations. Table 5 presents the maximum transient values of WMZ, henceforth called *peak WMZ*, for every single permeability layer, in the six stratified aquifers, during SWR. In the same table, the absolute (cm) and relative (%) differences between the peak WMZ and the quasi-steady state WMZ value at the conclusion of the experiment are documented. The last column of Table 5 depicts the time span (min) between the change in the hydraulic gradient, from 4 to 5 mm, and the moment in which peak WMZ was observed.

Peak WMZ values were, in general, larger for the low permeability layers, ranging between 0.79 and 1.37 cm, and smaller for the higher permeability strata (0.29–0.54 cm). Moreover, the relative position of each layer had a significant impact on the peak WMZ values since the strata closer to the impermeable aquifer bottom demonstrated the widest peak WMZ. This is evident by comparing the maximum WMZ values, for layers with the same permeability. In L-H-L aquifer, the lower (L) layer had a peak WMZ that was 57% bigger than peak WMZ in the upper (L) aquifer layer. Similarly, the peak WMZ of the lower (H) layer was 31% larger than the maximum WMZ value in the upper (H) stratum of the H-L-H experimental aquifer. The correlation between absolute ΔWMZ and the layer's permeability and relative position, was comparable to the relationship identified for the peak WMZ values.

The relative difference between the peak WMZ and the quasi-steady state WMZ, at the conclusion of the experiment, was negatively corelated to the layer's distance from the aquifer's top surface. In every single experimental aquifer, relative ΔWMZ was greater for the strata closer to the aquifer bottom and smaller for the layers further away from it, despite the impact of the permeability of each specific layer. So, even though peak WMZ for the upper (L) layer of the L-H aquifer was approximately 61% larger than peak WMZ in the lower (H) layer, the relative change between transient and quasi-steady state WMZ was twice that big for the bottom (H) layer. This demonstrated that the relative variation in WMZ values, even though affected by layer permeability, is mostly a function of the individual layer's relative position inside the heterogeneous aquifer.

Finally, a clear correlation was established between the layer's relative position, and the time in which the peak WMZ was observed. In all six stratified aquifers, widening occurred first in the lower strata, while significant time lagging, was observed for the layers closer to the aquifer's free surface. This time lagging, between the change of the hydraulic gradient and the corresponding peak WMZ, varied significantly from aquifer to aquifer, ranging from 15 up to 55 minutes. The observed time lagging in each hydrological system was in agreement with the total experimental time that was deemed necessary for the stabilization of the saline wedge (Table 1). In accordance with that, the shortest and longest time lags were observed in the lower layer of the H-L-H and H-M-L, and the upper layer of the H-L stratified aquifers, respectively, which were the laboratory aquifers in which the shortest (140 min) and the longest (180 min) laboratory measurements were conducted.
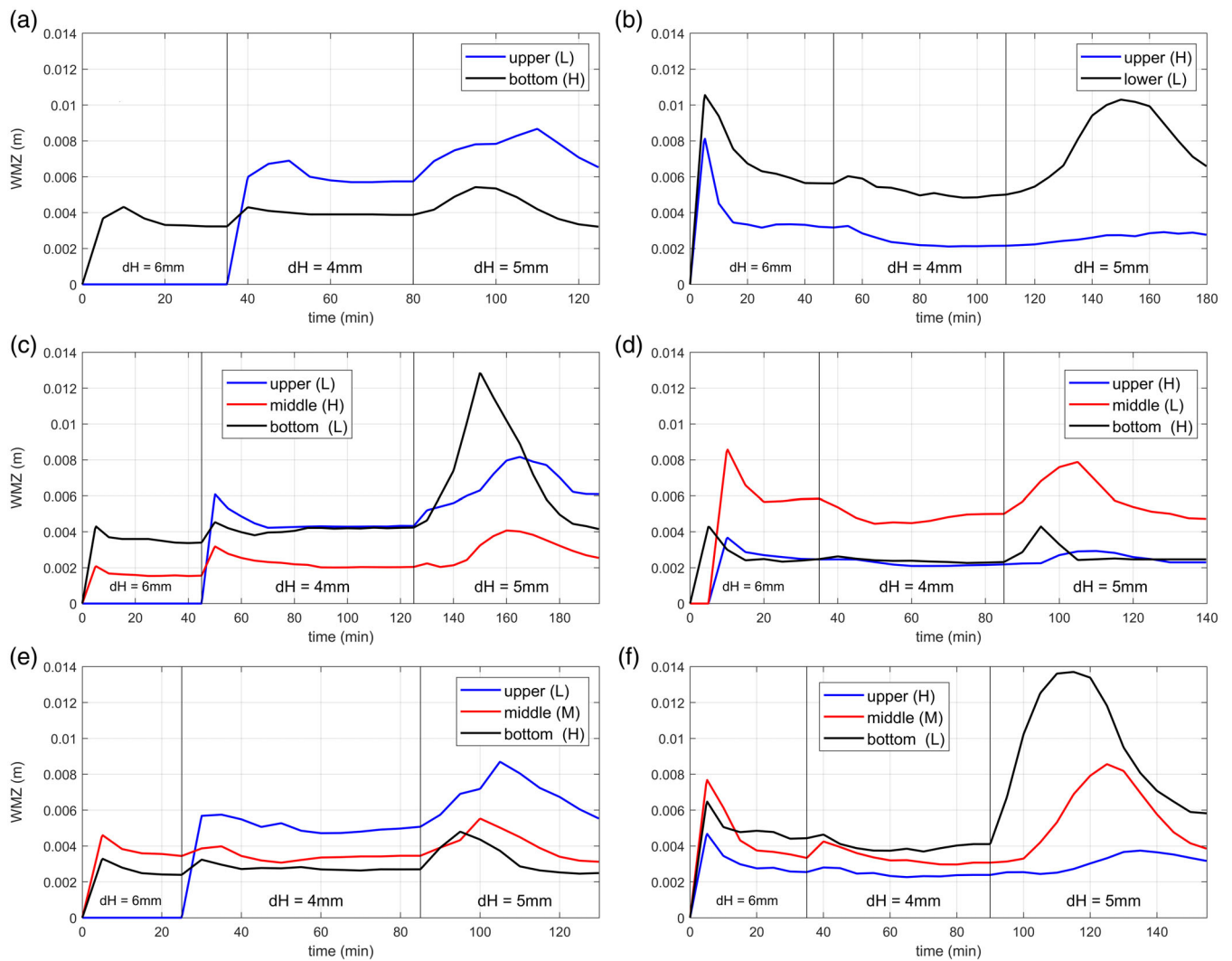
FIGURE 8 Experimental transient width of the mixing zone (WMZ) values of the (a) L-H, (b) H-L, (c) L-H-L, (d) H-L-H, (e) L-M-H and (f) H-M-L stratified aquifers

When the saline wedges are either under steady state or intrude further landwards, the velocity vector fields are comparable to those presented in Figure 6. In these cases, the groundwater flow inside and outside the saline wedges have opposing directions. Nevertheless, as Chang and Clement (2012) observed, during saltwater retreat, saltwater flow direction inside the saline wedge is reversed towards the sea. This temporary switch from an opposing to a unidirectional fluid flow regime, results in a highly disturbed flow field, which is responsible for the significant widening of the mixing zone observed in the current laboratory experiments. Since this switch occurs during the transient phase and gets reversed again as the system reaches steady state once more, peak WMZ values are generated for a limited time. Due the shape of the saltwater – freshwater interface, the effects of SWR occur first, and are more significant in the lower portion of the aquifer. Therefore, relative ΔWMZ is larger in the lowest aquifer strata. Similarly, peak WMZ values in the bottom strata are observed earlier than WMZ peaks in the upper-most layers.

4.1.3 | Angle of intrusion

The impact of stratification on the AOI was investigated for the first time in this study. The angle of intrusion is a parameter that vividly quantifies the orientation of the flow streamlines at the interface of the two liquids, freshwater and saltwater. Especially in the case of stratified systems, the permeability contrast between layers can lead to substantial flow line refraction at the boundaries, as shown in the previous sections, which in turn affects the saline intrusion front. Moreover, multiple experimental studies demonstrated that the presence of extremely low permeability or impermeable formations, like walls (Abdoulhalik et al., 2017), or high permeability zones, like fractures (Etsias et al., 2021) can significantly alter groundwater hydrodynamics and lead to unique shapes of intruding saline wedges. Nevertheless, to fully understand the hydrodynamics of more complex heterogeneity, decoding the basic mechanisms of SWI in more common heterogeneous setups, like the horizontal permeability layers of

TABLE 5 Quantification of transient WMZ characteristics during SWR experimental phase, for each permeability layer of the six investigated stratified aquifers

Aquifer	Layer	Peak WMZ (cm)	ΔWMZ (cm)	ΔWMZ (%)	Time-lag (min)
L-H	upper (L)	0.87	0.22	33.3	30
L-H	lower (H)	0.54	0.22	68.9	15
H-L	upper (H)	0.29	0.02	5.5	55
H-L	lower (L)	1.03	0.37	56.9	40
L-H-L	upper (L)	0.82	0.21	34.0	40
L-H-L	middle (H)	0.41	0.15	60.5	35
L-H-L	lower (L)	1.29	0.87	210.7	25
H-L-H	upper (H)	0.29	0.06	27.4	25
H-L-H	middle (L)	0.79	0.32	67.0	20
H-L-H	lower (H)	0.43	0.18	74.5	10
L-M-H	upper (L)	0.87	0.32	57.7	20
L-M-H	middle (M)	0.55	0.24	77.3	15
L-M-H	lower (H)	0.48	0.23	92.5	10
H-M-L	upper (H)	0.37	0.06	18.3	45
H-M-L	middle (M)	0.86	0.47	122.7	35
H-M-L	lower (L)	1.37	0.79	135.4	25

TABLE 6 Experimental AOI values for each permeability layer of the six heterogeneous aquifers, generated by a hydraulic head difference of 4 mm

Aquifer	Layer	AOI (°)
L-H	upper (L)	32.0
L-H	lower (H)	12.4
H-L	upper (H)	17.5
H-L	lower (L)	15.5
L-H-L	upper (L)	36.5
L-H-L	middle (H)	14.5
L-H-L	lower (L)	13.7
H-L-H	upper (H)	22.8
H-L-H	middle (L)	21.3
H-L-H	lower (H)	14.0
L-M-H	upper (L)	28.9
L-M-H	middle (M)	16.7
L-M-H	lower (H)	12.1
H-M-L	upper (H)	19.8
H-M-L	middle (M)	13.6
H-M-L	lower (L)	15.1

the study, is necessary. The current study of AOI constitutes a contribution towards this direction.

In general, the laboratory data demonstrated that saltwater-freshwater interface slope is mild in high permeability zones and steep in low permeability zones, this is in agreement with the numerical and laboratory investigations of Abarca (2006) and Robinson et al. (2016). The AOI values for the quasi steady-state conditions under dH = 4 mm, are presented in Table 6. The steepest angle of intrusion, equal to 32°, was observed in the upper layer of the L-H aquifer, while the mildest, AOI = 12.1°, in the bottom stratum of the H-L-H system. It has been well-established that in homogeneous aquifers (Figure 3 (a)-(c)) the saltwater—freshwater interface is not a straight line, but a curved one instead. Due to the curved shape of the intruding wedge, the angle of saline intrusion is expected to be much smaller towards the aquifer's impermeable bottom and greater closer to its open surface. Thus, the variation observed in AOI values for strata with the same permeability (L-H-L and H-L-H) can be attributed to the layer's vertical position inside the aquifer.

The permeability contrast between neighbouring strata resulted in a sharp alteration of AOIs at their interface; this was more evident in the L-H (ΔAOI = 19.6°) and the upper permeability boundaries of the L-H-L (ΔAOI = 22°) and L-M-H (ΔAOI = 12.2°) heterogeneous aquifers. To quantify this change, AOIs of the upper layers of the six heterogeneous aquifers were compared to the AOIs of equal permeability homogeneous aquifers at the same aquifer depth. Direct comparison with the AOIs for the whole of the homogeneous aquifers was avoided, since it would not take into account the impact of the strata's vertical position, thus failing to highlight the true impact of permeability contrast on the shape of the interface. It was observed that when a low permeability layer overlays a higher permeability zone, the angle of intrusion becomes steeper in that layer, while the opposite phenomenon occurs when a high permeability layer overlays a less permeable one. The largest changes in the values of AOI were observed in cases with higher $k_{contrast}$ (Figure 9). In the upper layer of the L-H-L aquifer the AOI was 24.5% larger than the angle of intrusion in the same section of the homogeneous L aquifer. Similarly, the absolute difference between the AOIs in the uppermost permeability layer of the HL stratified aquifer and the H homogeneous aquifer was equal to 25%. This phenomenon, similar to variations observed in experimental TL and WMZ values, can be attributed to streamline
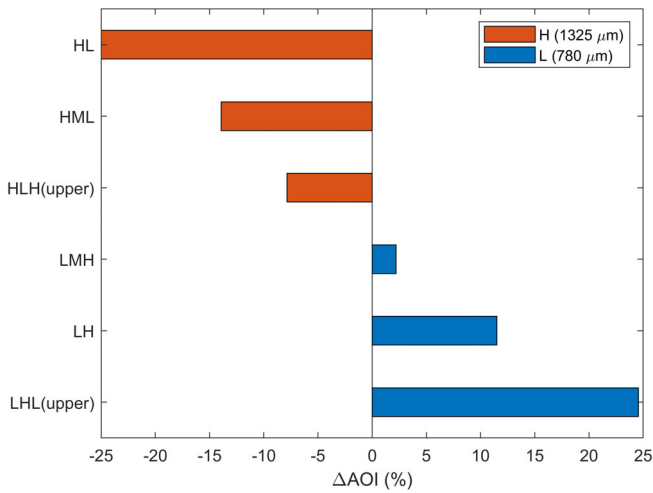
FIGURE 9 Experimental relative change of the angle of intrusion in higher (orange) and lower (blue) permeability upper layers of heterogeneous aquifers

refraction at the interface of the different permeability zones. The correlation between $k_{contrast}$ and ΔAOI was further investigated using numerical simulations (scenario 5).

The transient values of the AOI in the six stratified aquifers, during the whole duration of the experiment, are presented in Figure 10. During the initial intrusion of the saline wedge into a permeability layer, the saltwater-freshwater interface was the steepest while as the intrusion progressed further it became milder. The largest transient AOI was observed in the upper-most layer of the H-L aquifer (69.2°), while the bottom stratum in the LMH heterogeneous system had the mildest one (25.6°). The relative difference between the initial intruding AOI and the subsequent quasi steady state angle of intrusion, generated by dH = 6 mm, varied between 4.4% and 60.2%. Unlike what observed in the transient WMZ experimental data, apart from this initial phase of saline intrusion, the subsequent changes in the applied hydraulic head difference, dH = 6–4 mm and dH = 4–5 mm, were not followed by any sharp variation in the angle of intrusion, instead AOI gradually reached its steady state value. This indicates the peak WMZ values, identified
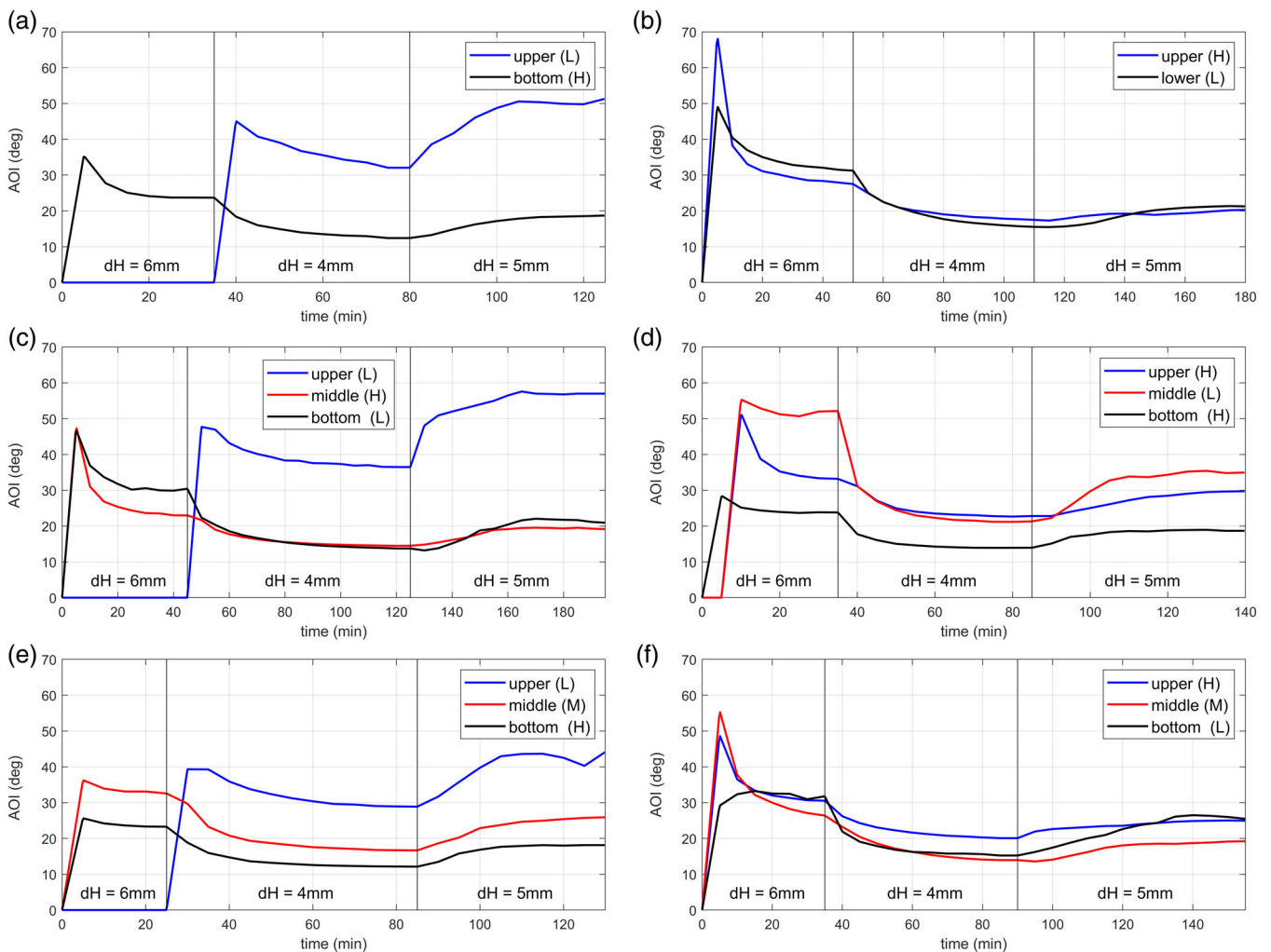

FIGURE 10 Experimental transient angle of intrusion (AOI) values of the (a) L-H, (b) H-L, (c) L-H-L, (d) H-L-H, (e) L-M-H and (f) H-M-L stratified aquifers

for SWR in the previous section, do not affect the orientation of the saltwater—freshwater interface. As expected, since the applied head difference is negatively correlated to the extent of saline intrusion (TL), dH was positively correlated to the steady state AOI values (Figure 10). In cases were just a small portion of the saline wedge intruded inside a layer, the resulting AOI was particularly sharp, like the ones observed in the upper-most layers of the L-H-L and L-M-H aquifers under dh = 5 mm (Figure 3(d),(e)).

4.1.4 | Critical head difference

In the experimental heterogeneous aquifers L-H, L-H-L and L-M-H (Figure 3(d), (f) and (h)) the saltwater wedge initiated by a head difference of 6 mm did not enter the upper, less-permeable layer. On the contrary the upper tip of the wedge was located at the interface of the two layers. This phenomenon was reproduced in the simulated models of the aforementioned laboratory aquifers (Figures A1d, A1f and A1h of the appendix). It was observed that given a specific $k_{contrast}$ between two layers, saltwater would not enter into the upper layer until a certain value of hydraulic head difference was applied to the system. This value, identified for the first time in this investigation, will be henceforth called critical head difference (dH_{crit}).

When a greater head difference (dH = 6 mm) is applied to the hydrological system, more freshwater flows into and subsequently out of the aquifer. Since in these L-H setups permeability is limited in the upper part of the aquifer, the outflow area widens incorporating parts of the more permeable lower zone. This confines the saline wedge inside the lower stratum. Only in cases when the inflow gets reduced to a sufficient level, can outflow occur strictly through the upper layer. At this point, saltwater intrudes in the upper portion of the aquifer.

These results could be important for multiple real-life applications. Intrusion of saltwater on the upper-most parts of freshwater aquifers negatively impacts soil quality thus affecting human activities such as farming (Alam et al., 2017). Moreover, one of the main variables influencing pumping induced saline intrusion is the absolute distance between the pumping wells and the saltwater—freshwater interface (Abdelgawad et al., 2018; Abdoulhalik & Ahmed, 2018b). Thus, being able to safely predict the pre-pumping distance of the saline front from the aquifer's free surface is a prerequisite for the successful management of actual coastal aquifers. The correlation between dH_{crit} and layer width and permeability was further quantified using numerical simulations (Scenario 6).

4.2 | Sensitivity analysis

4.2.1 | Sensitivity analysis Scenario 1 (effect of permeability contrast on the TL)

Six two-layered numerical models were created with varying $k_{contrast}$ values between their layers (Table A1 of the appendix). In half of these settings, a high permeability layer overlaid a lower permeability one
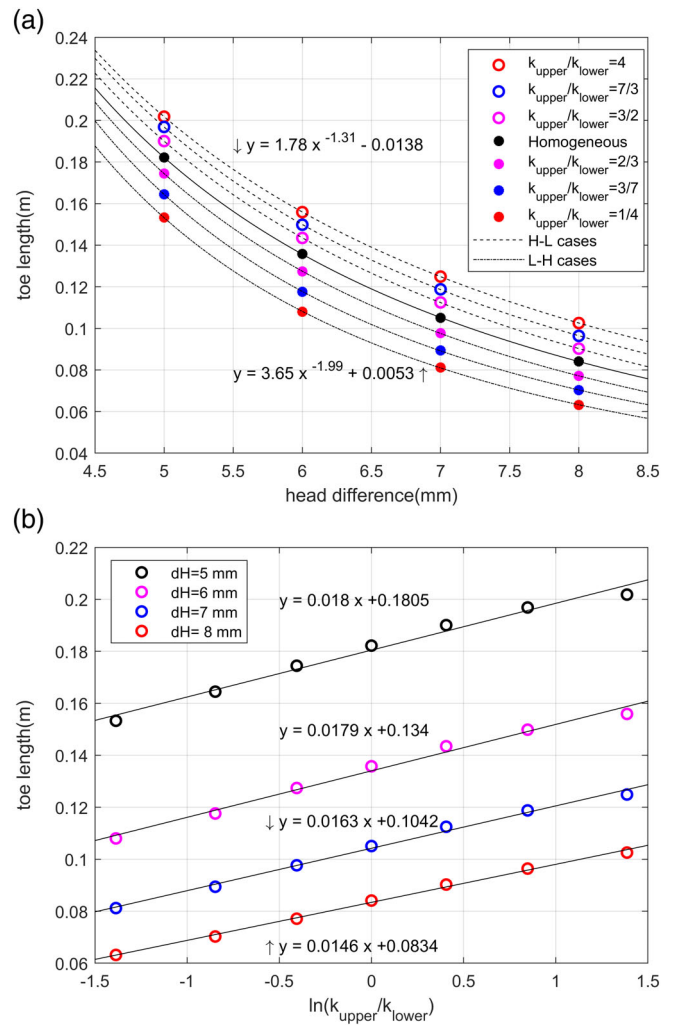

FIGURE 11 Impact of layer permeability contrast on the steady state toe length of saltwater wedge on simulated two-layered heterogeneous aquifers with the same average aquifer permeability (2.39×10^{-9} m^2). Toe length plotted against (a) head difference and (b) logarithm of $k_{contrast}$

(H-L cases), while in the remaining setups the upper layer permeability was lower (L-H cases). All simulated heterogeneous aquifers had the same average permeability, 2.39×10^{-9} m^2, which corresponded to the permeability of 1325 μm beads homogeneous aquifer. Four distinct head difference values (dH = 5, 6, 7 and 8 mm) were applied on the models. The calculated toe lengths are presented in Figure 11.

It was established that for equal total aquifer transmissivity, higher $k_{contrast}$ (k_{upper}/k_{lower}) corresponds to more extended saltwater intrusion while less permeable zones in the upper part of the aquifers drive more freshwater towards lower layers (Figure 6). The presence of more freshwater near the aquifers' bottom contributes to the seaward repulsion of the saline wedge. The smaller the value of $k_{contrast}$, as is the case in the low - high settings, the more intense is the containment of the saline wedge and vice versa. The toe length was negatively correlated to the applied head difference, while there was a linear relationship between toe length and the natural logarithm of $k_{contrast}$. The slopes in the linear equations of Figure 11(b) express the
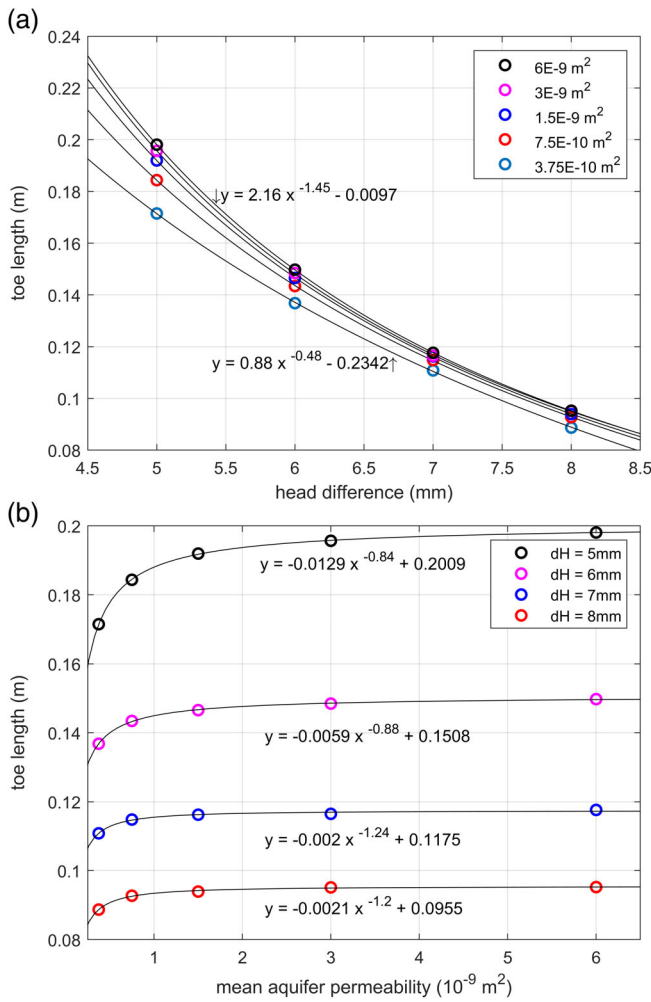
(a)

(b)

FIGURE 12 Impact of average aquifer permeability on the toe length of steady state saltwater wedge on two-layered heterogeneous aquifers with the same permeability contrast (k_{upper}/k_{low} = 2). Toe length plotted against (a) head difference and (b) average aquifer k

impact of $k_{contrast}$ to TL, while the second term represents the influence of the applied head difference. It is obvious that for smaller head differences the values of the slope tend to plateau (around 0.018 for the investigated aquifers) while the constant component gradually increases.

4.2.2 | Sensitivity analysis Scenario 2 (effect of total aquifer transmissivity on the TL)

Five two-layered numerical models were developed with varying average aquifer permeability but maintaining the same permeability contrast between their layers (k_{upper}/k_{lower} = 2) (Table A2 of the appendix). Saline intrusion was initiated by implementing the same values of hydraulic head difference with those applied in Scenario 1. The saltwater toe length was longer for higher average permeability aquifers, proving that TL in stratified aquifers is not only a function of $k_{contrast}$ between layers (Figure 12). Higher average permeability
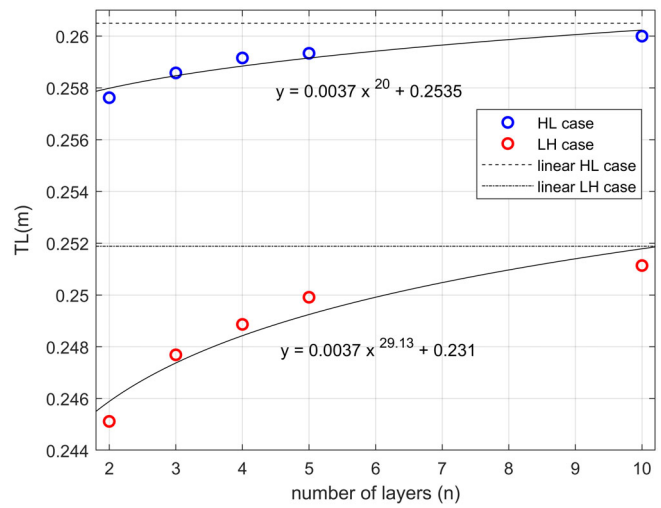

FIGURE 13 Impact of the number of heterogeneous layers on the toe length of the intruding wedge on simulated layered heterogeneous aquifers with the same average aquifer permeability (1.59×10^{-9} m^2). Highest layer permeability (H) equals to 2.39×10^{-9} m^2, while lowest layer permeability (L) is 7.98×10^{-10} m^2. Saltwater intrusion was initiated by a 4 mm hydraulic head difference

results in faster freshwater outflow from the upper part of the aquifer as observed in Figure 6. This leads to less suppression of the saline wedge, thus longer intrusion. Head difference and toe length were negatively correlated to each other, with a power ranging from −0.48 for the less permeable to −1.45 for the most permeable aquifer scenario. Correlation between toe length and mean aquifer permeability was a positive one (Figure 12(b)).

4.2.3 | Sensitivity analysis Scenario 3 (effect of the number of permeability layers on the TL)

In order to investigate the impact of the number of permeability layers on the length of intrusion, two sets of layered aquifers were simulated. In the first set, layer permeability decreased from top to bottom, while in the second one it increased. For each aquifer subset, aquifers of 2, 3, 5 and 10 heterogeneous layers were tested (Figures A2 and A3 of the appendix). In H-L cases the permeability of the upper most layer equaled to 2.39×10^{-9} m^2, while that of the lowest layer was 7.89×10^{-10} m^2, equal to the permeability of the experimental L homogeneous aquifer. The values of upper and lower layer permeabilities were reversed in the L-H set. The permeabilities of intermediate layers were derived via linear interpolation between the two uttermost permeability values. Total aquifer transmissivity was the same for all investigated aquifers (1.59×10^{-9} m^2).

The larger the number of layers, the longer saltwater intrusion extends for both aquifer subsets (Figure 13). When saltwater flows through two different permeability layers, flow refraction occurs at the layer boundary (Figure 4). The refraction angle depends on the permeability contrast between the layers (Lu et al., 2013). In

multilayered setups with smaller $k_{contrast}$ between them, the refraction of freshwater streamlines is limited. This contributes to a more linear saltwater-freshwater interface (Figure 3(h),(i)) and a faster outflow of freshwater towards the upper right part of the aquifer, thereby exacerbating SWI. Two extreme H-L and L-H cases were investigated. Permeability changed linearly from top to bottom between each one of the 110 element rows of the numerical model. TL was maximized in these setups and these values constituted the uppermost limit of the equations correlating toe length with the number of permeability layers.

The evaluation of experimental data, alongside a detailed sensitivity analysis, indicated that aquifer stratification significantly affects the length of intruding wedge; this is in agreement with previous studies (Abdoulhalik & Ahmed, 2017a; Lu et al., 2013). The study expanded the current knowledge, proving that the extend of saline intrusion in stratified systems is a multivariable problem, more complex than what previously hypothesized. In particular, TL in stratified systems is positively correlated to three different aquifer characteristics: the permeability contrast between layers, the total aquifer permeability and the number of different strata. Taking into account the

effect of all three aforementioned stratification characteristics is crucial in the successful evaluation of the physical extent of the intruding saltwater wedge length.

4.2.4 | Sensitivity analysis Scenario 4 (effect of permeability contrast on the steady-state WMZ)

This scenario was based on two-layered numerical models (Table A3 of the appendix). In the first model (Figure 14(a)) the WMZ of the upper layer was the target of the investigation while in the second subset of simulations (Figure 14(b)) it was that of the lower layer. The permeability of the investigated layer remained constant, while permeability values of the remaining layer varied to recreate different $k_{contrast}$ aquifers. L-H and H-L cases were investigated. WMZ values were plotted against the values of $k_{contrast}$. To better visualize the results of the investigation, $k_{contrast}$ equaled to k_{upper}/k_{lower} for the H-L aquifers, and to k_{lower}/k_{upper} for the L-H ones. This way, the two aquifer setups could be successfully presented in the same graph. The permeability of the target low-k layer equaled to 7.89×10^{-10} m^2 while that of the target high-k layer was 2.39×10^{-9} m^2. The widths of the mixing zone in the investigated layers were compared to the WMZ values for the equivalent homogeneous aquifers, that is, homogeneous aquifers having the exact same permeability with that of the layer investigated at every single case. This relative change in WMZ was calculated for all aquifers. It was established that the higher the $k_{contrast}$, the bigger the change in WMZ values. This change was far greater (10 to 30 times) when the investigated layer constituted the upper part of the aquifer. The results of sensitivity analysis corresponded well with the experimental data, where the greater WMZ changes occurred for the upmost permeability layers.
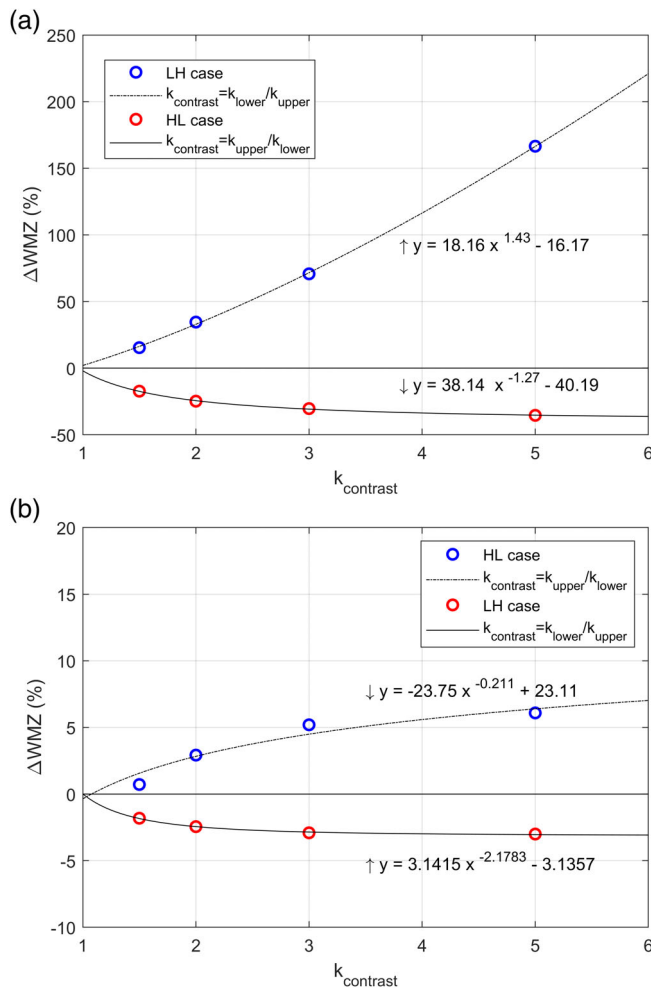

FIGURE 14 Impact of layer permeability contrast on the width of the mixing zone of the (a) upper and (b) lower layer of simulated two-layered heterogeneous aquifers
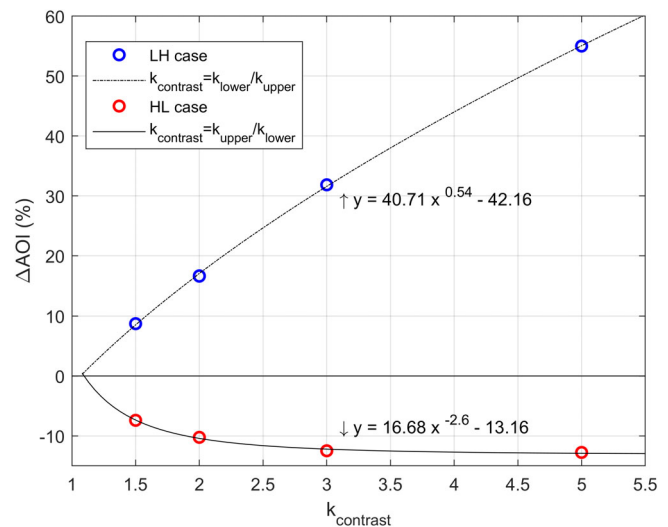

FIGURE 15 Impact of layer permeability contrast on the angle of intrusion on the upper layer of simulated two-layered heterogeneous aquifers
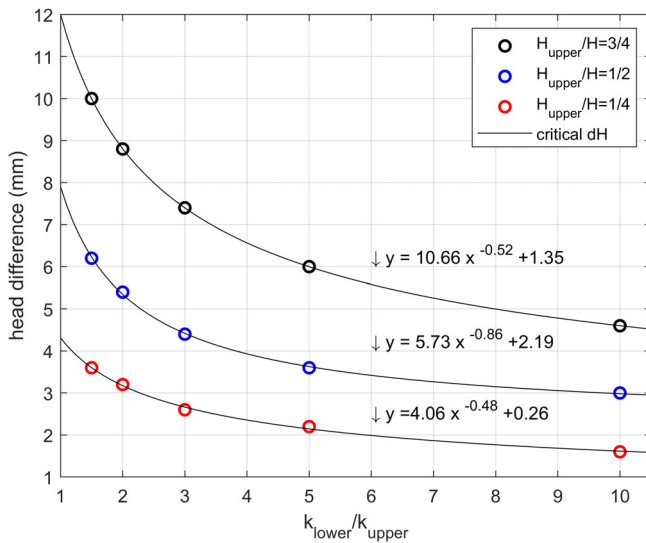
FIGURE 16 Impact of layer permeability contrast on the critical head difference for three distinct upper layer width setups, where the upper layer occupies ¼ (red), ½ (blue) or ¾ (black) of the total aquifer depth

4.2.5 | Sensitivity analysis Scenario 5 (effect of permeability contrast on the AOI)

Two distinct setups of two-layered aquifers representing L-H and H-L cases were simulated (Table A4 of the appendix). Permeability was kept constant in the upper layer, 7.89×10^{-10} m^2 for the L-H and 2.39×10^{-9} m^2 for the H-L subsets, while permeability in the lower layer was altered to recreate different values of $k_{contrast}$. Higher permeability contrast resulted in larger ΔAOI in both setups. The change was more radical on the L-H cases (up to six times). Relative AOI change maxed around $k_{upper} / k_{low} = 5$ for the H-L case, while the relationship between $k_{contrast}$ and ΔAOI resembled a linear one (power less than 2) for the L-H setup (Figure 15). Nevertheless, in cases with considerably higher permeability contrast on a L-H setup, saltwater would not intrude at all in the upper layer. These results constitute the first ever attempt of evaluating the impact of heterogeneity on the relatively understudied SWI characteristic of the angle of intrusion.

4.2.6 | Sensitivity analysis Scenario 6 (effect of layer width and permeability on the critical head)

Three setups of two-layered aquifers were simulated. In all cases a low permeability layer overlaid a higher permeability one. Upper layer permeability was kept constant equal to 7.89×10^{-10} m^2 while permeability of the lower layer was 1.5–10 times larger (1.19–7.89×10^{-9}). In each setup, the width of the upper layer varied such that it occupied ¾, ½ and ¼ of the total aquifer width. The layer permeability values of these numerical setups are presented in Table A5 of the appendix. It was found that the critical head difference was negatively correlated to $k_{contrast}$ in a similar way for all three cases (Figure 16). The width of the upper layer induced an important impact

on both first and third coefficient of the power law equation. This is the first study that defined this critical head difference and correlated its values with aquifer heterogeneity characteristics, such as the width of the different permeability strata and their permeability contrast.

5 | CONCLUSIONS

Laboratory measurements and numerical simulations were utilized to study the effect of aquifer stratification on saltwater intrusion characteristics. Head controlled saline intrusion was initiated into nine experimental aquifers by applying three distinct hydraulic gradients. As far as we know, this the most detailed laboratory study to date, investigating the effect of heterogeneity on SWI in coastal aquifers. Numerical simulations, using the SUTRA code, successfully reproduced the transient experimental data, for the two initial phases of saline intrusion and the final phase of saltwater retreat. The toe length of the intruding wedges, the width of mixing zone and the angle of intrusion were calculated through image analysis for all the test cases. Rigorous sensitivity analyses were then conducted using numerical simulations to explore the effect of additional layered configurations.

This study is the first ever sandbox investigation that presented transient experimental WMZ results on a heterogeneous aquifer setup, including an accurate quantification of experimental WMZ inside each individual layer of the stratified aquifers. Moreover, the correlation between aquifer stratification and the angle of saline intrusion was studied for the first time, while the novel concept of critical hydraulic head difference was identified through the analysis of the experimental data. Finally, the presented sensitivity analysis scenarios, were explicitly designed to quantify the impact of the various aquifer heterogeneity characteristics on SWI dynamics, in isolation from each other. The study's findings are presented in relation to each one of the specific SWI characteristics: TL, WMZ, AOI and critical dH.

Toe length

Three heterogeneity characteristics were identified as the ones with dominant effect on the length of intrusion, including the permeability contrast between layers, total aquifer transmissivity and the number of layers. The following conclusions were drawn:

- Heterogeneous aquifers with more permeable upper layers (H-L cases) exhibited the longest saltwater intrusion amongst layered aquifers with similar average permeability. A positive linear relationship correlated the logarithm of $k_{contrast}$ with the generated TL.
- In stratified aquifers with the same permeability contrast between layers, higher total aquifer transmissivity induced longer saltwater intrusion. The larger was the applied head difference, the smaller was the impact of transmissivity.
- In layered aquifers with the same $k_{contrast}$ and total aquifer transmissivity, the toe length was positively correlated to the number of permeability layers via a power law function. The upper limit of this

function was defined by the TL in systems were aquifer permeability changed linearly with depth.

These findings expand the established concept that TL in head-controlled stratified systems is a mere function of permeability contrast between strata (Shi et al., 2018). Instead, its relationship with aquifer stratification characteristics was proven to be much more complex than what was previously hypothesized.

Width of the mixing zone

- Expanding already established concepts about steady state WMZ, it was proven that when a lower permeability layer was either overlying or underlying higher permeability ones, its mixing zone was widened. On the other hand, WMZ was reduced in the case of the more permeable layer. The change in WMZ was positively correlated to $k_{contrast}$. Even though the identified WMZ variation was substantially greater for the overlying layer, the investigation proved that, this variation applies for all strata irrespectively of their relative vertical position in the aquifer, further expanding on the current concepts.
- Every change on the applied hydraulic head difference, was followed by an explicit transient widening of the mixing zone. This peak WMZ was considerably larger during the saltwater retreat phase of the experiments. Peak WMZ values were negatively correlated to each stratum's permeability, and to its vertical distance from the aquifers' impermeable bottom. Finally, the widening of the mixing zone was not instantaneous, instead a distinct time span was identified between the dH re-adjustment and the peak WMZ values. This time lagging was considerably longer for the uppermost permeability layers and shorter for the lower strata.

Angle of intrusion

- Experimental data revealed that the contrast between various permeability layers significantly altered the steady state values of AOI, especially in the upper part of the aquifers. In H-L setups, the AOI of the upper layer became smaller, while it increased in the inverse L-H cases. The relative change in AOI values was proportional to the permeability contrast between layers. Its effect being more significant in the L-H cases. This was the first time that the impact of stratification on AOI was quantified.
- At the point of initial intrusion of the saline wedge into an individual permeability layer, the transient saltwater—freshwater interface was up to 60% steeper than the interface's orientation after steady state was achieved. These steep AOI values, were negatively correlated to the layer's permeability, while they were observed only in the initial experimental phase and did not characterize any subsequent variations of the applied hydraulic gradient.

Critical head difference

- In cases were a low permeability layer overlaid more permeable aquifer structures, the saltwater wedge did not enter the top, less permeable layer. On the contrary it stabilized in its proximity, until a specific critical value of hydraulic head difference was applied to the system. This phenomenon, observed in three of the experimental stratified aquifers, was further investigated via numerical simulations. It was derived that the relationship between permeability contrast and critical head difference is an exponential formula, while the critical dH was negatively correlated to the width of the low permeability layer. Identifying this critical head difference and quantifying its relationship with stratification characteristics is the final novel contribution of the current study.

The current investigation outlined the impact of aquifer stratification on saltwater intrusion characteristics. Even though derived from an idealized two-dimensional laboratory setup, the novel conclusions of this study provide valuable insight on how realistic aquifer stratification could impact the main SWI characteristics, thus contributing towards the successful mitigation of the phenomenon. Although actual relationships between aquifer characteristics and the values of TL, WMZ and AOI were obtained via non-linear interpolation between the acquired numerical results, formulating generalized equations applicable in a wide variety of aquifer setups was beyond the scope of this work. Nevertheless, the presented findings could act as a solid foundation for future analytical studies in this direction. Finally, the detailed experimental data presented in this paper can be utilized in benchmarking models in upcoming numerical investigations of SWI in stratified coastal aquifers.

DATA AVAILABILITY STATEMENT
The data that support the findings of this study are available from the corresponding author upon reasonable request.

ORCID
Georgios Etsias https://orcid.org/0000-0002-6750-3994

REFERENCES
Abarca, E. (2006). *Seawater intrusion in complex geological environments*. UPC: Technical University of Catalonia.

Abarca, E., & Clement, T. P. (2009). A novel approach for characterizing the mixing zone of a saltwater wedge. *Geophysical Research Letters*, *36*(6), L06402. https://doi.org/10.1029/2008gl036995

Abdelgawad, A. M., Abdoulhalik, A., Ahmed, A. A., Moutari, S., & Hamill, G. (2018). Transient investigation of the critical abstraction rates in coastal aquifers: Numerical and experimental study. *Water Resources Management*, *32*(11), 3563–3577. https://doi.org/10.1007/s11269-018-1988-3

Abdoulhalik, A., Abdelgawad, A. M., & Ahmed, A. A. (2020). Impact of layered heterogeneity on transient saltwater upconing in coastal aquifers. *Journal of Hydrology*, *581*, 124393. https://doi.org/10.1016/j.jhydrol.2019.124393

Abdoulhalik, A., & Ahmed, A. A. (2017a). The effectiveness of cutoff walls to control saltwater intrusion in multi-layered coastal aquifers: Experimental and numerical study. *Journal of Environmental Management*, *199*, 62–73. https://doi.org/10.1016/j.jenvman.2017.05.040

Abdoulhalik, A., & Ahmed, A. A. (2017b). How does layered heterogeneity affect the ability of subsurface dams to clean up coastal aquifers contaminated with seawater intrusion? *Journal of Hydrology*, *553*, 708–721. https://doi.org/10.1016/j.jhydrol.2017.08.044

Abdoulhalik, A., & Ahmed, A. A. (2018a). Transience of seawater intrusion and retreat in response to incremental water-level variations. *Hydrological Processes*, *32*(17), 2721–2733. https://doi.org/10.1002/hyp.13214

Abdoulhalik, A., & Ahmed, A. A. (2018b). Transient investigation of saltwater upconing in laboratory-scale coastal aquifer. *Estuarine, Coastal and Shelf Science*, *214*, 149–160. https://doi.org/10.1016/j.ecss.2018.09.024

Abdoulhalik, A., Ahmed, A. A., & Hamill, G. A. (2017). A new physical barrier system for seawater intrusion control. *Journal of Hydrology*, *549*, 416–427. https://doi.org/10.1016/j.jhydrol.2017.04.005

Alam, M. Z., Carpenter-Boggs, L., Mitra, S., Haque, M. M. M., Halsey, J., Rokonuzzaman, M., Saha, B., & Moniruzzaman, M. (2017). Effect of salinity intrusion on food crops, livestock, and fish species at Kalapara coastal belt in Bangladesh. *Journal of Food Quality*, *2017*, 2045157. https://doi.org/10.1155/2017/2045157

Armanuos, A. M., Ibrahim, M. G., Mahmod, W. E., Takemura, J., & Yoshimura, C. (2019). Analysing the combined effect of Barrier Wall and freshwater injection countermeasures on controlling saltwater intrusion in unconfined coastal aquifer systems. *Water Resources Management*, *33*(4), 1265–1280. https://doi.org/10.1007/s11269-019-2184-9

Attanayake, P., & Sholley, M. (2007). Evaluation of the hydraulic gradient at an island for low-level nuclear waste disposal. Paper presented at the Symposium HS1001 at IUGG2007, Perugia.

Benson, C. H., Chiang, I., Chalermyanont, T., & Sawangsuriya, A. (2014). Estimating van Genuchten parameters α and n for Clean Sands from particle size distribution data. In *Soil behavior fundamentals to innovations in geotechnical engineering*. American Society of Civil Engineers.

Chang, Q., Zheng, T., Zheng, X., Zhang, B., Sun, Q., & Walther, M. (2019). Effect of subsurface dams on saltwater intrusion and fresh groundwater discharge. *Journal of Hydrology*, *576*, 508–519. https://doi.org/10.1016/j.jhydrol.2019.06.060

Chang, S. W., & Clement, T. P. (2012). Experimental and numerical investigation of saltwater intrusion dynamics in flux-controlled groundwater systems. *Water Resources Research*, *48*(9). https://doi.org/10.1029/2012WR012134

Dalai, C., Munusamy, S. B., & Dhar, A. (2020). Experimental and numerical investigation of saltwater intrusion dynamics on sloping sandy beach under static seaside boundary condition. *Flow Measurement and Instrumentation*, *75*, 101794. https://doi.org/10.1016/j.flowmeasinst.2020.101794

Dose, E. J., Stoeckl, L., Houben, G. J., Vacher, H. L., Vassolo, S., Dietrich, J., & Himmelsbach, T. (2014). Experiments and modeling of freshwater lenses in layered aquifers: Steady state interface geometry. *Journal of Hydrology*, *509*, 621–630. https://doi.org/10.1016/j.jhydrol.2013.10.010

Etsias, G., Hamill, G., Benner, E., Aguila, J. F., McDonnell, M., & Flynn, R. (2020). The effect of colour depth and image resolution on laboratory scale study of aquifer saltwater intrusion. Proceedings CERAI 27-28 August 2020. Part of ISBN 978-0-9573957-4-9.

Etsias, G., Hamill, G. A., Benner, E. M., Águila, J. F., McDonnell, M. C., Flynn, R., & Ahmed, A. A. (2020). Optimizing laboratory investigations of saline intrusion by incorporating machine learning techniques. *Water*, *12*(11), 2996. http://dx.doi.org/10.3390/w12112996

Etsias, G., Hamill, G. A., Campbell, D., Straney, R., Benner, E. M., Águila, J. F., McDonnell, M. C., Ahmed, A. A., & Flynn, R. (2021). Laboratory and numerical investigation of saline intrusion in fractured coastal aquifers. *Advances in Water Resources*, *149*, 103866. https://doi.org/10.1016/j.advwatres.2021.103866

Ferguson, G., & Gleeson, T. (2012). Vulnerability of coastal aquifers to groundwater use and climate change. *Nature Climate Change*, *2*(5), 342–345. https://doi.org/10.1038/nclimate1413

Goswami, R. R., & Clement, T. P. (2007). Laboratory-scale investigation of saltwater intrusion dynamics. *Water Resources Research*, *43*(4). https://doi.org/10.1029/2006wr005151

Guo, Q., Huang, J., Zhou, Z., & Wang, J. (2019). Experiment and numerical simulation of seawater intrusion under the influences of tidal fluctuation and groundwater exploitation in coastal multilayered aquifers. *Geofluids*, *2019*, 2316271. https://doi.org/10.1155/2019/2316271

Held, R., Attinger, S., & Kinzelbach, W. (2005). Homogenization and effective parameters for the Henry problem in heterogeneous formations. *Water Resources Research*, *41*(11). https://doi.org/10.1029/2004wr003674

Houben, G. J., Stoeckl, L., Mariner, K. E., & Choudhury, A. S. (2018). The influence of heterogeneity on coastal groundwater flow - physical and numerical modeling of fringing reefs, dykes and structured conductivity fields. *Advances in Water Resources*, *113*, 155–166. https://doi.org/10.1016/j.advwatres.2017.11.024

Kazakis, N., Pavlou, A., Vargemezis, G., Voudouris, K. S., Soulios, G., Pliakas, F., & Tsokas, G. (2016). Seawater intrusion mapping using electrical resistivity tomography and hydrochemical data. An application in the coastal area of eastern Thermaikos gulf, Greece. *Science of the Total Environment*, *543*, 373–387. https://doi.org/10.1016/j.scitotenv.2015.11.041

Ketabchi, H., Mahmoodzadeh, D., Ataie-Ashtiani, B., Werner, A. D., & Simmons, C. T. (2014). Sea-level rise impact on fresh groundwater lenses in two-layer small islands. *Hydrological Processes*, *28*(24), 5938–5953. https://doi.org/10.1002/hyp.10059

Konz, M., Ackerer, P., Meier, E., Huggenberger, P., Zechner, E., & Gechter, D. (2008). On the measurement of solute concentrations in 2-D flow tank experiments. *Hydrology and Earth System Sciences*, *12*(3), 727–738. https://doi.org/10.5194/hess-12-727-2008

Kuan, W. K., Jin, G., Xin, P., Robinson, C., Gibbes, B., & Li, L. (2012). Tidal influence on seawater intrusion in unconfined coastal aquifers. *Water Resources Research*, *48*(2). https://doi.org/10.1029/2011wr010678

Kuan, W. K., Xin, P., Jin, G., Robinson, C. E., Gibbes, B., & Li, L. (2019). Combined effect of tides and varying inland groundwater input on flow and salinity distribution in unconfined coastal aquifers. *Water Resources Research*, *55*(11), 8864–8880. https://doi.org/10.1029/2018WR024492

Lee, W.-D., Yoo, Y.-J., Jeong, Y.-M., & Hur, D.-S. (2019). Experimental and numerical analysis on hydraulic characteristics of coastal aquifers with seawall. *Water*, *11*(11). https://doi.org/10.3390/w11112343

Levanon, E., Gvirtzman, H., Yechieli, Y., Oz, I., Ben-Zur, E., & Shalev, E. (2019). The dynamics of sea tide-induced fluctuations of groundwater level and freshwater-saltwater Interface in coastal aquifers: Laboratory experiments and numerical modeling. *Geofluids*, *2019*, 6193134. https://doi.org/10.1155/2019/6193134

Li, X., Hu, B. X., Burnett, W. C., Santos, I. R., & Chanton, J. P. (2009). Submarine ground water discharge driven by tidal pumping in a heterogeneous aquifer. *Ground Water*, *47*(4), 558–568. https://doi.org/10.1111/j.1745-6584.2009.00563.x

Liu, S., Tao, A., Dai, C., Tan, B., Shen, H., Zhong, G., Lou, S., Chalov, S., & Chalov, R. (2017). Experimental study of tidal effects on coastal

groundwater and pollutant migration. *Water, Air, & Soil Pollution*, *228*(4), 163. https://doi.org/10.1007/s11270-017-3326-4

Liu, Y., Mao, X., Chen, J., & Barry, D. A. (2014). Influence of a coarse inter-layer on seawater intrusion and contaminant migration in coastal aquifers. *Hydrological Processes*, *28*(20), 5162–5175. https://doi.org/10.1002/hyp.10002

Lu, C., Chen, Y., Zhang, C., & Luo, J. (2013). Steady-state freshwater–seawater mixing zone in stratified coastal aquifers. *Journal of Hydrology*, *505*, 24–34. https://doi.org/10.1016/j.jhydrol.2013.09.017

McInnis, D., Silliman, S., Boukari, M., Yalo, N., Orou-Pete, S., Fertenbaugh, C., Sarre, K., & Fayomi, H. (2013). Combined application of electrical resistivity and shallow groundwater sampling to assess salinity in a shallow coastal aquifer in Benin, West Africa. *Journal of Hydrology*, *505*, 335–345. https://doi.org/10.1016/j.jhydrol.2013.10.014

Mehdizadeh, S. S., Werner, A. D., Vafaie, F., & Badaruddin, S. (2014). Vertical leakage in sharp-interface seawater intrusion models of layered coastal aquifers. *Journal of Hydrology*, *519*, 1097–1107. https://doi.org/10.1016/j.jhydrol.2014.08.027

Memari, S. S., Bedekar, V. S., & Clement, T. P. (2020). Laboratory and numerical investigation of saltwater intrusion processes in a Circular Island aquifer. *Water Resources Research*, *56*(2), e2019WR025325. https://doi.org/10.1029/2019WR025325

Na, J., Chi, B., Zhang, Y., Li, J., & Jiang, X. (2019). Study on the influence of seawater density variation on sea water intrusion in confined coastal aquifers. *Environmental Earth Sciences*, *78*(24), 669. https://doi.org/10.1007/s12665-019-8684-3

Noorabadi, S., Nazemi, A. H., Sadraddini, A. A., & Delirhasannia, R. (2017). Laboratory investigation of water extraction effects on saltwater wedge displacement. *Global Journal of Environmental Science and Management*, *3*(1), 21–32. https://doi.org/10.22034/gjesm.2017.03.01.003

Rathore, S. S., Zhao, Y., Lu, C., & Luo, J. (2018). Defining the effect of stratification in coastal aquifers using a new parameter. *Water Resources Research*, *54*(9), 5948–5957. https://doi.org/10.1029/2018WR023114

Robinson, G., Ahmed, A. A., & Hamill, G. A. (2016). Experimental saltwater intrusion in coastal aquifers using automated image analysis: Applications to homogeneous aquifers. *Journal of Hydrology*, *538*, 304–313. https://doi.org/10.1016/j.jhydrol.2016.04.017

Robinson, G., Hamill, G. A., & Ahmed, A. A. (2015). Automated image analysis for experimental investigations of salt water intrusion in coastal aquifers. *Journal of Hydrology*, *530*, 350–360. https://doi.org/10.1016/j.jhydrol.2015.09.046

Shen, Y., Xin, P., & Yu, X. (2020). Combined effect of cutoff wall and tides on groundwater flow and salinity distribution in coastal unconfined aquifers. *Journal of Hydrology*, *581*, 124444. https://doi.org/10.1016/j.jhydrol.2019.124444

Shi, W., Lu, C., Ye, Y., Wu, J., Li, L., & Luo, J. (2018). Assessment of the impact of sea-level rise on steady-state seawater intrusion in a layered coastal aquifer. *Journal of Hydrology*, *563*, 851–862. https://doi.org/10.1016/j.jhydrol.2018.06.046

Stoeckl, L., & Houben, G. (2012). Flow dynamics and age stratification of freshwater lenses: Experiments and modeling. *Journal of Hydrology*, *458-459*, 9–15. https://doi.org/10.1016/j.jhydrol.2012.05.070

Stoeckl, L., Houben, G. J., & Dose, E. J. (2015). Experiments and modeling of flow processes in freshwater lenses in layered Island aquifers: Analysis of age stratification, travel times and interface propagation. *Journal of Hydrology*, *529*, 159–168. https://doi.org/10.1016/j.jhydrol.2015.07.019

Stoeckl, L., Walther, M., & Morgan, L. K. (2019). Physical and numerical Modelling of post-pumping seawater intrusion. *Geofluids*, *2019*, 7191370. https://doi.org/10.1155/2019/7191370

Strack, O. D. L., & Ausk, B. K. (2015). A formulation for vertically integrated groundwater flow in a stratified coastal aquifer. *Water Resources Research*, *51*(8), 6756–6775. https://doi.org/10.1002/2015WR016887

Strack, O. D. L., Stoeckl, L., Damm, K., Houben, G., Ausk, B. K., & de Lange, W. J. (2016). Reduction of saltwater intrusion by modifying hydraulic conductivity. *Water Resources Research*, *52*(9), 6978–6988. https://doi.org/10.1002/2016WR019037

Sweijen, T., Aslannejad, H., & Hassanizadeh, S. M. (2017). Capillary pressure–saturation relationships for porous granular materials: Pore morphology method vs. pore unit assembly method. *Advances in Water Resources*, *107*, 22–31. https://doi.org/10.1016/j.advwatres.2017.06.001

Takahashi, M., Momii, K., & Luyun, R. (2018). Laboratory scale investigation of dispersion effects on saltwater movement due to cutoff wall installation. *E3S Web Conference*, *54*, 38. Retrieved from. https://doi.org/10.1051/e3sconf/20185400038

van Genuchten, M. T. (1980). A closed-form equation for predicting the hydraulic conductivity of unsaturated soils. *Soil Science Society of America Journal*, *44*(5), 892–898. https://doi.org/10.2136/sssaj1980.03615995004400050002x

Vithanage, M., Engesgaard, P., Jensen, K. H., Illangasekare, T. H., & Obeysekera, J. (2012). Laboratory investigations of the effects of geologic heterogeneity on groundwater salinization and flush-out times from a tsunami-like event. *Journal of Contaminant Hydrology*, *136-137*, 10–24. https://doi.org/10.1016/j.jconhyd.2012.05.001

Voss, C., & Provost, A. (2010). SUTRA—A model for saturated–unsaturated, Variabledensity ground-water flow with solute or energy transport. *Water-Resources Investigations Report* (02–4231).

Voss, C., & Souza, W. R. (1987). Variable density flow and solute transport simulation of regional aquifers containing a narrow freshwater-saltwater transition zone. *Water Resources Research*, *23*(10), 1851–1866. https://doi.org/10.1029/WR023i010p01851

Ward, J. D., Simmons, C. T., & Dillon, P. J. (2008). Variable-density modelling of multiple-cycle aquifer storage and recovery (ASR): Importance of anisotropy and layered heterogeneity in brackish aquifers. *Journal of Hydrology*, *356*(1), 93–105. https://doi.org/10.1016/j.jhydrol.2008.04.012

Weinstein, Y., Burnett, W. C., Swarzenski, P. W., Shalem, Y., Yechieli, Y., & Herut, B. (2007). Role of aquifer heterogeneity in fresh groundwater discharge and seawater recycling: An example from the Carmel coast, Israel. *Journal of Geophysical Research C: Oceans*, *112*(C12). https://doi.org/10.1029/2007JC004112

Yu, X., Xin, P., & Lu, C. (2019). Seawater intrusion and retreat in tidally-affected unconfined aquifers: Laboratory experiments and numerical simulations. *Advances in Water Resources*, *132*, 103393. https://doi.org/10.1016/j.advwatres.2019.103393

Zhang, Q., Volker, R. E., & Lockington, D. A. (2002). Experimental investigation of contaminant transport in coastal groundwater. *Advances in Environmental Research*, *6*(3), 229–237. https://doi.org/10.1016/S1093-0191(01)00054-5

SUPPORTING INFORMATION

Additional supporting information may be found online in the Supporting Information section at the end of this article.